PHYSICAL REVIEW D **81,** 014004 (2010)

Study of Higgs boson production and its $b\bar{b}$ decay in γ-γ processes in proton-nucleus collisions at the LHC

David d'Enterria[1] and Jean-Philippe Lansberg[2,3,*]

[1]*ICC-UB and ICREA, Universitat de Barcelona, 08028 Barcelona, Catalonia*
[2]*Centre de Physique Théorique, École Polytechnique, CNRS, 91128 Palaiseau, France*
[3]*SLAC National Accelerator Laboratory, Theoretical Physics, Stanford University, Menlo Park, California 94025, USA*

(Received 30 September 2009; published 7 January 2010)

We explore for the first time the possibilities to measure an intermediate-mass ($m_H =$ 115–140 GeV/c^2) standard model Higgs boson in electromagnetic proton-lead (pPb) interactions at the CERN Large Hadron Collider (LHC) via its $b\bar{b}$ decay. Using equivalent Weizsäcker-Williams photon fluxes and Higgs effective field theory for the coupling $\gamma\gamma \to H$, we obtain a leading-order cross section of the order of 0.3 pb for exclusive Higgs production in elastic ($p\mathrm{Pb} \xrightarrow{\gamma\gamma} XH\mathrm{Pb}$) and semielastic ($p\mathrm{Pb} \xrightarrow{\gamma\gamma} XH\mathrm{Pb}$) processes at $\sqrt{s_{NN}} = 8.8$ TeV. After applying various kinematics cuts to remove the main backgrounds ($\gamma\gamma \to b\bar{b}$ and misidentified $\gamma\gamma \to q\bar{q}$ events), we find that a Higgs boson with $m_H =$ 120 GeV/c^2 could be observed in the $b\bar{b}$ channel with a 3σ significance integrating 300 pb^{-1} with an upgraded pA luminosity of 10^{31} cm^{-2} s^{-1}. We also provide for the first time semielastic Higgs cross sections, along with elastic $t\bar{t}$ cross sections, for electromagnetic pp, pA and AA collisions at the LHC.

DOI: 10.1103/PhysRevD.81.014004 PACS numbers: 14.80.Bn, 25.20.Lj

I. INTRODUCTION

The standard model (SM) of particle physics predicts the existence of a scalar Higgs particle (H) to explain the breaking of the electroweak gauge symmetry observed in nature [1]. Direct searches for the Higgs boson at the LEP collider have constrained its mass above 114.4 GeV/c^2 at 95% confidence level (CL) [2], and global fits to precision electroweak data exclude $m_H > 154$ GeV/c^2 at 95% CL [3]. Yet, it turns out that the favored intermediate-mass range above the LEP limit is the most difficult region for Higgs searches in pp collisions at the LHC. Indeed, for $m_H < 135$ GeV/c^2, the dominant decay mode is $H \to b\bar{b}$ with a typical cross section $\sigma(H \to b\bar{b}) \approx 30$ pb at $\sqrt{s} =$ 14 TeV [4], which is overwhelmed by the combinatorial background from QCD b-jets production with $\sigma(b\bar{b}) \approx$ 500 μb. As a matter of fact, the $H \to b\bar{b}$ decay channel is now considered unaccessible[1] at the LHC [7,8], and testing the expected mass-dependent Yukawa coupling of the Higgs boson to the b quark seems to be left open to study only at a next e^+e^- linear collider. In the intermediate-mass range, standard Higgs searches need thus to resort either to rare decay modes such as $H \to \gamma\gamma$ or to very stringent cuts on the final-state particles, which lead to 3–4 orders of magnitude reduction of the observed cross section.

In this context, the clean topologies of *exclusive* Higgs production in "peripheral" pp processes mediated by colorless exchanges—such as two gluons in a color-singlet state (Pomerons) [9,10] or two photons [9,11]—are attracting increasing interest [12,13] despite their much smaller cross sections, $\mathcal{O}(10^{-4}$–$10^{-5})$, compared to the dominant gluon-fusion or vector-boson-fusion (VBF) Higgs production channels. Exclusive events are characterized by wide rapidity gaps on both sides of the singly produced central system and the survival of both protons scattered at very low angles with respect to the beam. The final state is thus much cleaner with just the decaying products in the central detector, the signal/background is much more favorable than in parton-parton interactions, and the event kinematics can be constrained measuring the final protons with near-beam detectors in the LHC tunnel [14].

In this work we consider Higgs production from γ-γ collisions, also known as ultraperipheral collisions (UPCs) [15], with proton and ion beams at the LHC. All charges accelerated at high energies generate electromagnetic fields which, in the equivalent photon approximation (EPA) [16], can be considered as (quasireal) photon beams[2] [17]. A significant fraction of the pp [13,14] and PbPb [18] collisions at the LHC will involve for the first time γ-induced interactions at TeV energies with effective photon luminosities never reached before. The highest available photon energies are of the order of the inverse Lorentz contracted radius R of the source charge, $\omega_{\max} \approx \gamma/R$. The photon spectrum is thus harder for smaller charges, which favors proton over nuclear beams in the production of heavy particles. However, since the photon flux scales as the squared charge of the beam, Z^2, two-photon cross sections are extremely enhanced for ion

[*]Present address at École Polytechnique (Palaiseau).

[1]There are however recent developments [5,6] that give some hope in the $WH(b\bar{b})$ and $ZH(b\bar{b})$ associated production modes.

[2]The emitted photons are almost on mass shell, with virtuality $-Q^2 < 1/R^2$, where R is the radius of the charge, i.e. $Q \approx$ 0.28 GeV for protons ($R \approx 0.7$ fm) and $Q < 0.06$ GeV for nuclei ($R_A \approx 1.2A^{1/3}$ fm) with mass number $A > 16$.

 © 2010 The American Physical Society

beams ($Z^4_{\rm Pb} = 5 \cdot 10^7$ for lead-lead). Particle production in two-photon interactions at hadronic colliders has been studied at RHIC by PHENIX [19] and STAR [20,21], and at the Tevatron by CDF [22–24]. They are also part of the ALICE [25,26], ATLAS [27,28], CMS [29,30], and LHCb [31,32] physics programmes with proton and/or nuclear beams. Two-photon fusion favors the production of spinless resonances ($\gamma\gamma \to$ vector is forbidden by the Landau-Yang theorem). In this work, we propose to exploit the photon fluxes generated by both the proton and Pb ions at the LHC to study the possible production of the SM Higgs boson. Higgs photon-fusion production in proton or nucleus collisions at TeV energies is not a new idea (see e.g. [33] for references). Pioneering calculations for pp [34] and PbPb [35–37] collisions, updated more recently [9,38–40], predict cross sections of a SM Higgs boson with $m_H = 120$ GeV/c^2 in the $\sigma_{pp\to\gamma\gamma\to H} = 0.1$ fb and $\sigma_{\rm PbPb\to\gamma\gamma\to H} = 10$ pb ranges, respectively. Unfortunately, the small value of the pp cross section and the large event pileup[3] in pp collisions on the one hand, and the very low design luminosities expected for PbPb, on the other, preclude any real measurement of the Higgs boson in those channels.

Our proposal to study $\gamma\gamma \to H$ in pA collisions presents advantages with respect to both ultraperipheral AA and pp collisions. First, compared to AA, one benefits from (i) beam luminosities more than 4 orders of magnitude larger: $\mathcal{L}_{p\rm Pb} \sim 10^{31}$ cm^{-2} s^{-1} versus $\mathcal{L}_{\rm PbPb} \sim 10^{27}$ cm^{-2} s^{-1}; (ii) higher beam-beam c.m. energies: $\sqrt{s_{NN}} = 8.8$ TeV compared to 5.5 TeV; (iii) higher $\gamma\gamma$ c.m. energies (harder proton photon spectrum and smaller distance of approach between the centers of the radiating charges); and (iv) easy removal of other photoproduction backgrounds characterized in the AA case by additional photon exchanges which lead to forward neutron(s) emission. The net result is that one can reach higher masses and yields for any centrally produced system H. The advantage with respect to pp UPCs is threefold: (i) a Z^2 increase in one of the photon fluxes, and the possibilities (ii) to trigger on and carry out the measurement with almost no pileup, and (iii) to remove most of the exclusive diffractive backgrounds—since the nucleus is a fragile object, Pomeron-mediated interactions in pA will, at variance with pp, almost always lead to the emission of a few nucleons detectable in the zero-degree calorimeters.

In the following, we present a detailed generator-level study for the exclusive $p{\rm Pb}\overset{\gamma\gamma}{\to}pH{\rm Pb}$ (elastic) and $p{\rm Pb}\overset{\gamma\gamma}{\to}XH{\rm Pb}$ (semielastic) processes (Fig. 1), obtained with the MADGRAPH code supplemented with nuclear equivalent photon spectra. We compute the tree-level SM cross sections for the signal—in the Higgs effective field theory (HEFT) approximation—and for the expected backgrounds. We determine the expected yields in a 1-year run taking into account the maximum attainable pPb luminosities. We then discuss the reconstruction of the $H \to b\bar{b}$ decay for a Higgs boson with $m_H = 120$ GeV/c^2, including the trigger and analysis cuts needed to minimize the backgrounds. After accounting for basic detector reconstruction effects (b-jet misidentification, $b\bar{b}$-jets invariant mass resolution), we determine the expected statistical significance of the measurement. Our results are promising in various fronts. First, they indicate that the study of the difficult $H - b$-quark coupling could be accessible in this production mode at the LHC. Second, the observation of the $\gamma\gamma \to H$ process provides an independent measurement of the Higgs-γ coupling (likely measured previously in the traditional $H \to \gamma\gamma$ discovery channel). The $\gamma\gamma$-Higgs cross section is generated at the one-loop level by all heavy charged particles (W and top quark in the SM) and is thus sensitive to possible contributions of new charged particles with masses beyond the energy covered directly by the collider: e.g. via chargino and top-squark loops in supersymmetric (SUSY) extensions of the SM.

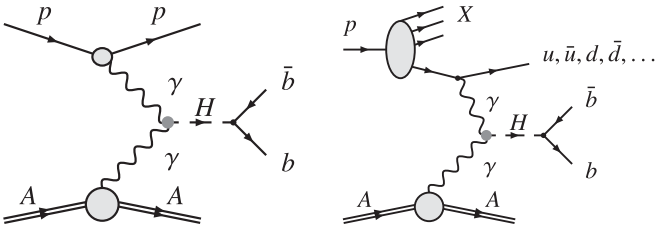

(a) Elastic case (b) Semielastic case

FIG. 1. Feynman diagrams for two-photon collisions with proton and nucleus beams producing a Higgs boson decaying into $H \to b\bar{b}$. (a) Elastic production (both photons are emitted coherently and the proton and nucleus survive). (b) Semielastic production (the photon from the proton is emitted by a quark, the proton subsequently breaks up).

II. CROSS SECTION EVALUATION

The cross section for a two quasireal photon process in hadronic collisions to produce a final state H at center-of-mass (c.m.) energy $W_{\gamma\gamma}$ (e.g. a particle H with mass m_H, see Fig. 1), factorizes into the product of the elementary cross section for $\gamma\gamma \to H$ convoluted with the equivalent photon spectra from the two colliding beams:

$$\sigma(AB\overset{\gamma\gamma}{\to}AHB) = \int d\omega_1 d\omega_2 \frac{f_{\gamma/A}(\omega_1)}{\omega_1}\frac{f_{\gamma/B}(\omega_2)}{\omega_2} \times \sigma(\gamma\gamma \to H(W_{\gamma\gamma})), \quad (1)$$

where ω_1 and ω_2 are the two photon energies, and $f_{A,B}(\omega)$ are the photon fluxes at energy ω emitted by the hadrons A and B. The photon energies determine the c.m. energy

[3] *Pileup* refers to the overlapping events occurring in the same bunch crossing at high luminosity $\mathcal{L}$. For the nominal pp running at $\mathcal{L} = 10^{34}$ cm^{-2} s^{-1} one expects about 25 simultaneous collisions at the LHC.

TABLE I. Relevant parameters for photon-induced processes in AB collisions at the LHC: (i) beam luminosity, $\mathcal{L}_{AB}$, (ii) nucleon-nucleon c.m. energy, $\sqrt{s_{NN}}$, (iii) beam energies, $E_{\rm beam}$, (iv) Lorentz factor, $\gamma = \sqrt{s_{NN}}/(2m_N)$, (v) effective radius (of the largest species), R_A, (vi) photon "cutoff energy" in the c.m. frame, $\omega_{\rm max}$, (vii) maximum photon-nucleon c.m. energy, $\sqrt{s_{\gamma_N}^{\rm max}} = \sqrt{2\omega_{\rm max} m_N}$, (viii) maximum photon-photon c.m. energy, $\sqrt{s_{\gamma\gamma}^{\rm max}}$, and (ix) hadronic cross section, $\sigma_{\rm inel}$ (the pp value is from [41], the pA and AA geometric cross sections are obtained with a Glauber model with $\sigma_{{\rm inel},NN} \approx 80$ mb [42]).

System	$\sqrt{s_{NN}}$ (TeV)	$\mathcal{L}_{AB}$ ($\rm cm^{-2}\,s^{-1}$)	$E_{\rm beam1} + E_{\rm beam2}$ (TeV)	γ	R_A (fm)	$\omega_{\rm max}$ (GeV)	$\sqrt{s_{\gamma_N}^{\rm max}}$ (GeV)	$\sqrt{s_{\gamma\gamma}^{\rm max}}$ (GeV)	$\sigma_{\rm inel}$ (mb)
pp	14	10^{34}	7 + 7	7455	0.7	2450	8400	4500	110
pO	9.9	$2.7 \cdot 10^{30}$	7 + 3.5	5270	3.0	340	2600	690	480
pAr	9.4	$1.5 \cdot 10^{30}$	7 + 3.15	5000	4.1	240	2130	480	830
pPb	8.8	$1.5 \cdot 10^{29}$	7 + 2.76	4690	7.1	130	1500	260	2160
OO	7.0	$2 \cdot 10^{29}$	3.5 + 3.5	3730	3.0	240	1850	490	1500
ArAr	6.3	$0.6 \cdot 10^{29}$	3.15 + 3.15	3360	4.1	160	1430	320	2800
PbPb	5.5	$5 \cdot 10^{26}$	2.76 + 2.76	2930	7.1	80	950	160	7700

$W_{\gamma\gamma} = \sqrt{s_{\gamma\gamma}} = \sqrt{4\omega_1\omega_2}$ and the rapidity y of the produced system:

$$\omega_{1,2} = \frac{W_{\gamma\gamma}}{2} e^{\pm y}, \quad \text{and} \quad y = 0.5 \ln(\omega_1/\omega_2). \qquad (2)$$

For symmetric systems, the maximum effective two-photon energy $W_{\gamma\gamma}^{\rm max}$ occurs at $y = 0$, when $\omega_1^{\rm max} = \omega_2^{\rm max} \approx \gamma/b_{\rm min}$, where $\gamma = \sqrt{s_{NN}}/(2m_N)$ is the Lorentz relativistic factor[4] and $b_{\rm min} \approx 2R_A$ the minimum separation between the two charges of radius R_A. Note that these "maximum" photon energies do not have to be interpreted as a hard cutoff but as an indication of the energy ($\omega > \gamma\beta/b$) from which the photon flux is exponentially suppressed.

Table I summarizes the most relevant parameters for ultraperipheral pp, pA, and AA collisions at the LHC [18,43]. It has to be noted that whereas proton-proton and nucleus-nucleus collisions are obviously part of the approved baseline physics programme of the LHC, proton-nucleus collisions are still considered as an upgrade of the heavy-ion programme [43,44]. Detailed studies [44] have nonetheless shown that is a perfectly feasible mode of operation of the collider, and its physics possibilities have been discussed vastly in the literature as a crucial baseline for the interpretation of the AA data [43,45,46]. At the LHC, protons and ions have to travel in the same magnetic lattice[5] i.e. the two beams have to have the same charge-to-mass ratio Z/A. This limits the beam momentum of a given species to $p = 7$ TeV Z/A for the nominal 8.3 T dipole bending field. Thus, the energy in the nucleon-nucleon center-of-mass is $\sqrt{s_{NN}} = 14\ {\rm TeV}\sqrt{(Z_A Z_B)/(AB)}$. In the case of AB collisions with asymmetric beam energies the rapidity of the c.m. system shifts relative to the laboratory by $\Delta y_{\rm c.m.} = 0.5 \ln[(Z_A B)/(Z_B A)]$. Thus, for pA collisions the rapidity shifts span a range of $\Delta y_{\rm c.m.} = 0.35$–$0.47$ for ions from oxygen to lead. For $\gamma\gamma$ processes in ultraperipheral pA collisions, the average rapidity shift is even larger due to the harder EPA spectrum from the proton (e.g. $\langle \Delta y \rangle \approx 1.7$ for the case of 120 GeV/c^2 Higgs boson, see Sec. IV). The quoted pA luminosities have to be considered as unofficial but plausible values (see Sec. III C). The Table indicates that the maximum $\gamma\gamma$ c.m. energies attainable range from $\sqrt{s_{\gamma\gamma}^{\rm max}} \approx 160$ GeV for PbPb to 4.5 TeV for pp (obtained taking $R_p = 0.7$ fm). Two-photon fusion collisions in pPb have $\sqrt{s_{\gamma\gamma}^{\rm max}} \approx 260$ GeV, i.e. more than twice the most probable mass of the SM Higgs boson.

A. Equivalent photon fluxes

In the Weizsäcker-Williams approximation [16], the flux of equivalent photons from a relativistic particle of charge Z is determined from the Fourier transform of its electromagnetic field. For an extended charge with form factor $F(Q^2)$, such as a proton or a nucleus, the energy spectrum $f_{\gamma/A}(x) = dn_\gamma/dx$, where $x = \omega/E$ is the fraction of the beam energy carried by the photon, can be calculated from [47]:

$$f_{\gamma/A}(x) = \frac{\alpha Z^2}{\pi} \frac{1 - x + 1/2x^2}{x} \times \int_{Q^2_{\rm min}}^{\infty} \frac{Q^2 - Q^2_{\rm min}}{Q^4} |F(Q^2)|^2 dQ^2, \qquad (3)$$

where $\alpha = 1/137$, and Q^2 is the 4-momentum transfer squared from the charge. The minimum momentum transfer squared, $Q^2_{\rm min} \approx (x m_A)^2/(1 - x)$, is a function of x and the mass m_A of the projectile.

For UPCs involving ions it is more appropriate to calculate the spectrum of equivalent photons as a function of impact parameter [48,49]. The photon energy spectrum

[4] $m_N = 0.9315$ GeV/c^2 for nuclei, and $m_p = 0.9383$ GeV/c^2 for protons.

[5] The magnetic rigidity is defined as $p/Z = Br$ for an ion with momentum p and charge Z that would have a bending radius r in a magnetic field B.

produced by a charge Z sweeping past a target, integrated on the impact parameter b from $b_{\min}$ to infinity, is a textbook analytical result [50]:

$$f_{\gamma/A}(x) = \frac{\alpha Z^2}{\pi}\frac{1}{x}[2x_i K_0(x_i)K_1(x_i) - x_i^2(K_1^2(x_i) - K_0^2(x_i))], \tag{4}$$

where $x_i = x m_N b_{\min}$, and K_0, K_1 are the modified Bessel functions of the second kind of zero and first order, related, respectively, to the emission of longitudinally and transversely polarized photons. The transverse polarization dominates for ultrarelativistic particles ($\gamma \gg 1$). Although this approach treats the nucleus as an idealistic hard sphere, the use of more realistic Woods-Saxon profiles gives effective $\gamma\gamma$ luminosities only about 5% lower [51] than the hard-sphere approximation in the range of c.m. energies $W_{\gamma\gamma} \approx 0.5 W_{\gamma\gamma}^{\max}$ dominant in the exclusive production of an intermediate-mass Higgs boson.

The figure of merit for $\gamma\gamma$ processes in UPCs is $\mathcal{L}_{\gamma\gamma}^{\text{eff}} \equiv \mathcal{L}_{AB} d\mathcal{L}_{\gamma\gamma}/dW_{\gamma\gamma}$, where $\mathcal{L}_{AB}$ is the collider luminosity for a given AB system and $d\mathcal{L}_{\gamma\gamma}/dW_{\gamma\gamma}$ is the photon-photon luminosity as a function of the $\gamma\gamma$ c.m. energy obtained integrating the two photon fluxes over all rapidities y, $d^2\mathcal{L}_{\gamma\gamma}/dW_{\gamma\gamma}dy = (2/W_{\gamma\gamma}) f_{\gamma/A}(W_{\gamma\gamma}/2e^{y}) f_{\gamma/B}(W_{\gamma\gamma}/2e^{-y})$. For illustration, in Fig. 2 we show $\mathcal{L}_{\gamma\gamma}^{\text{eff}}$ obtained from the parametrization of Ref. [48] of $d\mathcal{L}_{\gamma\gamma}/dW_{\gamma\gamma}$ for ion-ion collisions and using the $\mathcal{L}_{AB}$ luminosities quoted[6] in Table I. The curves are computed for the elastic $\gamma\gamma$ fluxes. Inclusion of the semielastic fluxes would yield luminosities twice higher, as we discuss later. For comparison, we also plot the effective $\gamma\gamma$ luminosities in e^+e^- collisions at the ILC ($\mathcal{L}_{e+e-} = 2 \cdot 10^{34}$ cm^{-2} s^{-1}) for $\sqrt{s} = 250$ GeV and 500 GeV [52].

The elastic pPb two-photon luminosities at the LHC are similar to those for PbPb for low $\gamma\gamma$ center-of-mass energy, $W_{\gamma\gamma}$, and become higher for $W_{\gamma\gamma} > 50$ GeV due to the larger pPb beam energies. For energies of interest for an intermediate-mass Higgs (dotted vertical line in Fig. 2), both $\gamma\gamma$ luminosities are still almost 2 order of magnitude lower than that in proton-proton collisions. However, as we discuss in Sec. III C, there are seemingly no technical reasons that would prevent one to increase the instantaneous proton-nucleus luminosity by up to a factor $\mathcal{O}(60)$ (third curve in Fig. 2). We remark that our study, based on MADGRAPH, does not make direct use of the effective two-photon luminosities plotted in Fig. 2, although it gives similar results for the fluxes as we explain below.

1. Elastic production ($pA \xrightarrow{\gamma\gamma} pHA$)

In the case of high-energy protons, the equivalent photon spectrum can be obtained from its elastic form factors in the dipole approximation, $F_M = G_M^2$ and $F_E = (4m_p^2 G_E^2 + Q^2 G_M^2)/(4m_p^2 + Q^2)$ with $G_E^2 = G_M^2/\mu_p^2 = (1 + Q^2/Q_0^2)^{-4}$, where $Q_0^2 \approx 0.71$ GeV^2 and $\mu_p^2 \approx 7.78$, and reads [47]

$$f_{\gamma/p}(x) = \frac{dn_\gamma}{dx} = \frac{\alpha}{\pi}\frac{1-x}{x} \times [\varphi(x, Q_{\max}^2/Q_0^2) - \varphi(x, Q_{\min}^2/Q_0^2)], \quad \text{where} \tag{5}$$

$$\varphi(x, Q) = (1 + ay)\left[-\ln\frac{1+Q}{Q} + \sum_{k=1}^{3}\frac{1}{k(1+Q)^k}\right] + \frac{(1-b)y}{4Q(1+Q)^3} + c\left(1 + \frac{y}{4}\right) \times \left[\ln\frac{(1+Q)-b}{1+Q} + \sum_{k=1}^{3}\frac{b^k}{k(1+Q)^k}\right] \tag{6}$$

with $y = x^2/(1-x)$. The parameters a, b, and c are given by $a = (1+\mu_p^2)/4 + 4m_p^2/Q_0^2 \approx 7.16$, $b = 1 - 4m_p^2/Q_0^2 \approx -3.96$, and $c = (\mu_p^2 - 1)/b^4 \approx 0.028$. This flux,[7] with $Q_{\max}^2 \approx \mu_F^2$, is implemented in the standard version of MADGRAPH V.4 [53]. The use of more rigorous expressions e.g. including the magnetic dipole moment of the proton [54] results only on small differences in the final EPA fluxes [55].

In UPCs involving nuclei one could imagine, starting from Eq. (4), to compute the two photon flux by simple multiplication and identifying $b_{\min}$ with the radii of the two

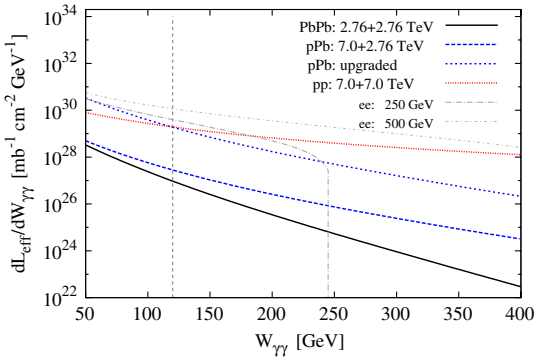

FIG. 2 (color online). Effective elastic two-photon luminosities $\mathcal{L}_{AB}(d\mathcal{L}_{\gamma\gamma}/dW_{\gamma\gamma})$ for pp, pPb and PbPb collisions at the LHC based on the beam luminosities quoted in Table I. For pPb we show also the curve corresponding to a $\times 60$ luminosity upgrade (Sec. III C). The effective $\gamma\gamma$ luminosities in e^+e^- collisions at the ILC are also shown for $\sqrt{s} = 250$ GeV and 500 GeV (thin dashed lines) [52].

[6]We note, as pointed out in [52], that the $\mathcal{L}_{\gamma\gamma}^{\text{eff}}$ plot (Fig. 3) of [18], does not use correct (updated) values for $\mathcal{L}_{pp}$ at the LHC.

[7]The precise value of $Q_{\max}^2$ does not actually matter since the flux is already negligible for Q^2 larger than 2 GeV^2.

TABLE II. Production cross sections for a SM Higgs boson with $m_H = 120$ GeV/c^2 (total and for the $H \to b\bar{b}$ decay) in elastic ($AB \xrightarrow{\gamma\gamma} AHB$) ultraperipheral collisions for the LHC colliding systems listed in Table I. For pp and pA UPCs, we also quote the semielastic ($AB \xrightarrow{\gamma\gamma} XHB$) cross sections (with the kinematical cuts $|y_{q'}| > 2.5$ and $p_T^{q'} < 5$ GeV/c for the radiating quark).

System	$\sqrt{s_{NN}}$ (TeV)	$\sigma(\gamma\gamma \to H)$ elastic (pb) [$m_H = 120$ GeV/c^2]		$\sigma(\gamma\gamma \to H)$ semielastic (pb) [$m_H = 120$ GeV/c^2]	
		H total	$H \to b\bar{b}$	H total	$H \to b\bar{b}$
pp	14	$0.18 \cdot 10^{-3}$	$0.13 \cdot 10^{-3}$	$0.59 \cdot 10^{-3}$	$0.45 \cdot 10^{-3}$
pO	9.9	$3.5 \cdot 10^{-3}$	$2.5 \cdot 10^{-3}$	$4.9 \cdot 10^{-3}$	$3.5 \cdot 10^{-3}$
pAr	9.4	$1.3 \cdot 10^{-2}$	$9.7 \cdot 10^{-3}$	$1.7 \cdot 10^{-2}$	$1.4 \cdot 10^{-2}$
pPb	8.8	0.17	0.12	0.16	0.12
OO	7.0	$3.7 \cdot 10^{-2}$	$2.6 \cdot 10^{-2}$		
ArAr	6.3	0.37	0.26		
PbPb	5.5	18	13		

nuclei A and B for each for photon flux. However, we would then miss geometrical constraints in order to have the two photons produced at the same point, outside the nuclei while the nuclear "halos" do not overlap. In an AB collision this implies requiring not only $b_1 > R_A$, $b_2 > R_B$, but also $|\vec{b}_1 - \vec{b}_2| > R_A + R_B$. The latter condition, which excludes any overlapping configurations, prevents to derive a factorized formula for the $\gamma\gamma$ flux in terms of the momentum fraction x_1 and x_2 carried by each photon from their parents nuclei in Eq. (4). Photon fluxes are encoded in MADGRAPH in the same way as any parton distribution and one has to use factorized expressions. One option to overcome those complications, as proposed by Cahn [56], would be to impose $b_1 > R_A + R_B$, $b_2 > R_A + R_B$ which together always exclude overlaps. However, this leads to quite pessimistic estimates of the joint flux [48] since it prevents configurations where the two nucleus are very close and produce very energetic $\gamma\gamma$ collisions. An alternative is simply not to exclude overlaps and to impose $b_1 > R_A$ and $b_2 > R_B$ alone, i.e. to use Eq. (4) for both fluxes. As discussed in [48], in such a case, the deviation from an exact evaluation of the flux basically depends on the ratio of the invariant mass of the $\gamma\gamma$ system over the c.m. energy. For the production of a Higgs with $m_H = 120$ GeV/c^2 in PbPb collisions at the LHC, one expects a deviation of a factor of 2. This is by far the most extreme case since the Pb nuclei are large and the available energy is reduced forcing the $\gamma\gamma$ creation point to be very near the nuclei, including overlapping configurations. For ArAr and OO collisions, the corrections are already much smaller [48]. A comparison of the cross sections which we obtain with factorized fluxes without full nonoverlap condition (see later Table II, third column) with the results for those systems using the exact nonoverlap condition [40] confirms the small impact of the approximations used here.

In the pA case, using Eq. (4) with $b_2 > R_A$ and Eq. (5) is in fact not problematic since (i) the available energy is higher than in AA UPCs, (ii) the overlap between the proton and the nucleus A is reduced by the small size of the proton ($R_p \approx 0.7$ fm),[8] and (iii) on average, the photon radiated by the proton (for which $b_{\min} \simeq 0.7$ fm) is much more energetic.[9] As a consequence, the $\gamma\gamma$ production point is typically far from the nucleus surface and the proton cannot overlap with the latter. Quantitatively, we have found that the photon momentum fraction from a Pb nucleus in a pPb collisions is typically below 0.015, corresponding to $b_2 \gtrsim 2R_{\rm Pb}$. Therefore, in our calculations, we have used the equivalent photon spectrum given by Eq. (5) for protons and by Eq. (4) for ions with the requirement $b_{\min} = R_A$, where the effective nuclear radii are obtained in the standard way from their mass number A via $R_A = r_0 A^{1/3}$ with $r_0 = 1.2$ fm. As discussed above, in practice this condition, along with the proton flux, ensures that the final state is produced *exclusively* and outside of the colliding system pA, i.e. it avoids the hadronic overlap and breakup of the colliding beams. The fact that our $\gamma\gamma$ cross sections agree well with other recent calculations [9,40] (see later) lends support to our approximations.

2. Semielastic production ($p\mathrm{A} \xrightarrow{\gamma\gamma} XHA$)

In semielastic production, Fig. 1(b), the proton does not radiate coherently. The photon flux is generated by its quarks and is followed by the proton breakup. As found previously [59–61] for two-photon fusion processes in pp collisions, we expect in the pA case a comparable magnitude of the incoherent photon flux ($\propto A = 1$) emitted by the quarks compared to the flux from coherent elastic emission ($\propto Z^2 = 1$). The same is not true for UPCs involving two nuclei where the elastic contribution clearly

[8] Of course, the proton is not a sphere and its radius is not a well-defined quantity. Effectively, electron-proton scattering fits yield a charge rms-radius $R_p = 0.89 \pm 0.2$ fm [57], and diffractive results at HERA indicate an effective proton transverse size $R_p = 0.65 \pm 0.2$ fm [58].

[9] Hence the larger shift in the rapidity distribution of a particle X in $p\mathrm{A} \xrightarrow{\gamma\gamma} X$ compared to hadronic $p\mathrm{A} \to X$ collisions (see later).

dominates over the semielastic one (either from the constituent protons or quarks of the nuclei) due to the large Z^2 factor in both coherent fluxes. For semielastic $pA \xrightarrow{\gamma\gamma} XHA$ collisions, one can consider the proton flux as a partonic distribution $\gamma^p(x, Q^2)$, the photon being the parton, where x denotes the momentum fraction of the "inelastic" photon in the proton and Q^2 the resolution scale at which the proton is probed. It can be approximated by [59,60,62]

$$\gamma^p(x, Q^2) = \frac{\alpha}{2\pi} \log\frac{Q^2}{Q_0^2} \sum_q \int_x^1 \frac{dy}{y} P_{\gamma q}(x/y) \times [q(y, Q^2) + \bar{q}(y, Q^2)] \quad (7)$$

with $P_{\gamma q}(z) = e_q^2(1 + (1 - z)^2)/z$, Q_0^2 an energy cutoff, and $q(x, Q^2)$ the quark PDFs in the proton. An improved expression was further discussed in [63]. In our work, we shall take advantage of MADGRAPH features and generate the semielastic contribution by considering the partonic processes $q\gamma \to qH \to qb\bar{b}$ (where $q = u, \bar{u}, d, \bar{d}, s, \bar{s}$ are all possible radiating light quarks) convoluted with the quark PDFs in the proton[10] and the photon flux from the nucleus A. The contributions from all the light quarks but the u are found to amount to $1/3$ of the u quark alone, since they are comparatively suppressed by their smaller PDFs in the proton and/or by their lower quark charge.

Obviously, one has to introduce an effective mass for the quark otherwise the cross section would be logarithmically divergent as Eq. (7) is if Q_0^2 is set to 0. We take this effective mass to be $\hat{m}_q = 300$ MeV. In order to limit the off shellness of the quasireal photon, we have also found reasonable to bound the maximum transverse momentum of the outgoing quark to $p_{T,\max}^{q'} = 5$ GeV/c. This provides us at the same time with a natural value for the factorization scale entering the PDF for the incoming quark, $Q^2 = (p_{T,\max}^{q'})^2$.

In the semielastic class of events, hadrons from the fragmentation of the radiating quark and from the proton remnants spray in the proton-direction hemisphere, while a pure γ beam, unaccompanied by hadronic activity, is generated by the nucleus in the opposite hemisphere. To guarantee a wide enough rapidity gap as expected in exclusive production, we exclude events where the jet initiated by the radiating quark q' ends up in the central region. All our semielastic cross sections are thus computed with the condition $|y_{q'}| > 2.5$.

B. $\gamma\gamma \to H$ coupling (Higgs effective field theory)

The coupling of the scalar Higgs to photons is mostly mediated by W- and top-quark loops. The HEFT model [65], where the Higgs boson couples directly to photons, can be used as an approximation of the standard model. For a not too heavy ($m_H < 2m_t$) and not very energetic ($p_T <$ $2m_t$) Higgs, it is a good approximation to take the mass of the heavy quark in the loop to infinity. In the limit of small Higgs masses—below about $m_H = 150$ GeV/c^2 which satisfies $m_H^2/(4m_W^2) \lesssim 1$—the loop induced interaction can be approximately described by the Lagrangian

$$\mathcal{L}_{\gamma\gamma H}^{\text{eff}} = -\frac{1}{4} g F_{\mu\nu} F_{\mu\nu} H, \quad (8)$$

where $F_{\mu\nu} = \partial_\mu A_\nu - \partial_\nu A_\mu$ is the photon field strength tensor. Because of the Abelian nature of QED there is only one effective vertex g between photons and Higgs bosons. The value for the coupling constant in the HEFT model as implemented in MADGRAPH [53] is given by

$$g = -\frac{\alpha}{\pi v}\frac{47}{18}\left(1 + \frac{66}{235}\tau_w + \frac{228}{1645}\tau_w^2 + \frac{696}{8225}\tau_w^3 + \frac{5248}{90475}\tau_w^4 + \frac{1280}{29939}\tau_w^5 + \frac{54528}{1646645}\tau_w^6 - \frac{56}{705}\tau_t - \frac{32}{987}\tau_t^2\right),$$

where $\tau_t = m_H^2/(4m_t^2)$ and $\tau_w = m_H^2/(4m_W^2)$. Higher order τ_t and τ_w terms have been neglected.

III. RESULTS I: CROSS SECTIONS AND RATES

We employ the MADGRAPH V.4 Monte Carlo [53] with the elastic and semielastic proton photon fluxes discussed in the previous section together with the nucleus photon flux Eq. (4) and the HEFT model for the Higgs-photon coupling, Eq. (8), to compute the Higgs boson cross sections in two-photon fusion processes for the systems of Table I. The Higgs decay branching ratio to $b\bar{b}$ is obtained in MADGRAPH with HDECAY [66], e.g. BR($H \to b\bar{b}$) $\approx$ 72% for $m_H = 120$ GeV/c^2. We compute also the SM cross sections for the exclusive production of $b\bar{b}$ and (possibly misidentified) $c\bar{c}$ and light-quark (u, d, s) pairs, which constitute the most important physical background for the measurement of the $H \to b\bar{b}$ channel.

A. Signal cross sections: $\gamma\gamma \to H$

Table II lists the cross sections for Higgs ($m_H =$ 120 GeV/c^2) production in photon-photon collisions for the systems tabulated in Table I. In Fig. 3 we show our predictions for the SM Higgs production cross sections as a function of m_H for the same systems. For $m_H =$ 120 GeV/c^2, the cross sections span a range from 0.18 fb for pp up to 18 pb for PbPb. Compared to pPb collisions, the ratios of the Higgs cross section between the different systems are roughly pp:pO:pAr:pPb:PbPb = 1/900:1/50:1/13:1:100. It is thus apparent that the large photon flux of the lead ion (Z^2) largely compensates for the higher projectile energies of the proton or light-ion beams, as well as the largest photon energies attainable with the smaller species. However, when one takes into account the much smaller maximum luminosities at reach in the PbPb

[10] We have used CTEQ6L.1 [64].

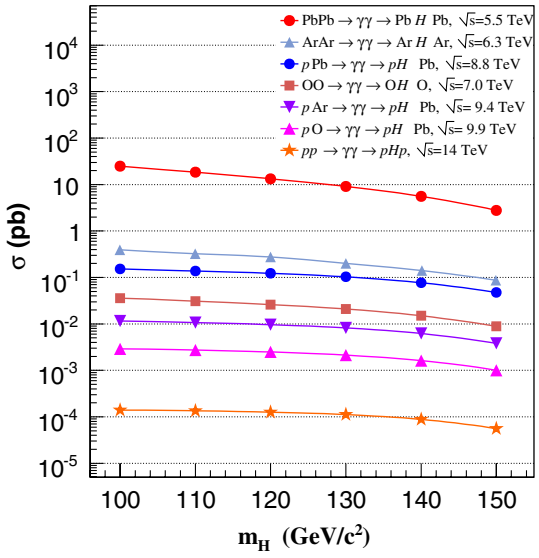

FIG. 3 (color online). Cross sections for the exclusive production of the SM Higgs versus its mass m_H in elastic ultraperipheral nucleus-nucleus, proton-nucleus, and proton-proton collisions at the LHC (systems listed in Table I).

running mode, such an advantage completely disappears (see Sec. III C).

The values we have obtained for the elastic exclusive Higgs cross sections for pp and AA (those for pA are published in this work for the first time) agree well with those found in the recent literature [9,40] except for the PbPb case where we overpredict the cross section by a factor two compared to [40] due to the absence of the exact nonoverlap condition in the convolution of fluxes as discussed previously. For pp, the calculation of Khoze *et al.* [9] makes use of the standard formula for a narrow $\gamma\gamma$ resonance of spin J: $\sigma(\gamma\gamma \to H) = 8\pi^2(2J+1)\Gamma(H \to \gamma\gamma)/m_H^3\delta(1 - m^2/m_H^2)$, which yields $\sigma(\gamma\gamma \to H) \simeq 0.12$ fb, for $m_H = 120$ GeV/c^2 with width $\Gamma(H \to \gamma\gamma) \simeq 7.9$ keV/c^2 [66]. This result takes into account a $\gamma\gamma$ luminosity of $1.1 \cdot 10^{-3}$ and a gap-survival factor of $\hat{S}^2 = 0.9$, encoding the probability to produce fully exclusively the Higgs without any other hadronic activity from soft rescatterings between the protons.

The signal cross sections are enhanced by a factor of 2 by allowing for semielastic configurations where only the nucleus remains intact but the proton breaks apart after the photon emission from one of its quarks (see right columns of Table II). This is the first time, as far as we can tell, that semielastic UPC Higgs cross sections appear in the literature. As a cross-check, we have compared the semielastic cross sections for high-mass dileptons in pp UPCs obtained with our MADGRAPH prescription (see Sec. II A 2) with the results of [61] finding a good agreement. Note that in the pp case the cross sections are multiplied by a factor of 2 since there are two possibilities (one for each proton) to emit the photon and fragment. For pPb, we find a Higgs cross sections for semielastic $\gamma\gamma$ production, where the photon is radiated directly from the quarks of the proton, of $\sigma(p\text{Pb} \to \gamma\gamma \to XH\text{Pb}) \approx 0.16$ fb, i.e. very similar to that of coherent exclusive production. We do not quote the semielastic cross sections for nucleus-nucleus UPCs since in these cases the photon flux, emitted either from their constituent protons or quarks, is much smaller than the coherent one.

B. Background cross sections: $\gamma\gamma \to b\bar{b}$, $c\bar{c}$, $q\bar{q}$

The main background to the $H \to b\bar{b}$ process is the continuum production of $b\bar{b}$ and misidentified $c\bar{c}$ and $q\bar{q}$ ($q = u, d, s$) dijets. Table III quotes the exclusive $Q\bar{Q}$ and $q\bar{q}$ cross sections in the range of invariant masses $m_{\text{inv}} =$ 100–140 GeV/c^2 relevant for a Higgs peak at 120 GeV/c^2 expected to be smeared by the b-jet reconstruction resolution (see Sec. IV D). Without any kinematical cut the combined $b\bar{b}$ continuum cross sections over $\Delta m =$ 40 GeV/c^2 is about 25 times larger (e.g. $\sigma_{b\bar{b}} = 8$ pb for pPb) than the Higgs cross section at 120 GeV/c^2 (see Table II) for all systems.

As we will see below, such irreducible background can be safely reduced with a few kinematics cuts. The $c\bar{c}$ ($q\bar{q}$)

TABLE III. Production cross sections for exclusive production of $b\bar{b}$, $c\bar{c}$, and $q\bar{q}$ ($q = u, d, s$) with $m_{\text{inv}} =$ 100–140 GeV/c^2 and for $t\bar{t}$ (all masses) in elastic ($AB \xrightarrow{\gamma\gamma} Aq\bar{q}B$) ultraperipheral collisions for the LHC colliding systems listed in Table I. For pp and pA UPCs, we also quote the semielastic ($AB \xrightarrow{\gamma\gamma} Xb\bar{b}B$, with $|y_{q'}| > 2.5$ and $p_T^{q'} < 5$ GeV/c for the photon-emitting quark) cross sections.

System	$\sqrt{s_{NN}}$ (TeV)	$\sigma(\gamma\gamma \to b\bar{b})$ (pb) [$m_{b\bar{b}} =$ 100–140 GeV/c^2]		$\sigma(\gamma\gamma \to c\bar{c})$ (pb) [$m_{c\bar{c}} =$ 100–140 GeV/c^2]	$\sigma(\gamma\gamma \to q\bar{q})$ (pb) [$m_{q\bar{q}} =$ 100–140 GeV/c^2]	$\sigma(\gamma\gamma \to t\bar{t})$ (pb) [all $m_{t\bar{t}}$]
		Elastic	Semielastic	Elastic	Elastic	Elastic
pp	14	$3.4 \cdot 10^{-3}$	$1.1 \cdot 10^{-2}$	$7.9 \cdot 10^{-2}$	0.2	$0.36 \cdot 10^{-3}$
pO	9.9	$6.8 \cdot 10^{-2}$	$9.5 \cdot 10^{-2}$	1.6	3.9	$2.7 \cdot 10^{-3}$
pAr	9.4	0.27	0.36	6.1	15.8	$8.1 \cdot 10^{-3}$
pPb	8.8	3.4	4.5	78	200	$6.2 \cdot 10^{-2}$
OO	7.0	0.75		17	39	$3.9 \cdot 10^{-2}$
ArAr	6.3	7.6		170	400	$1.0 \cdot 10^{-2}$
PbPb	5.5	420		$9.4 \cdot 10^3$	$2.5 \cdot 10^4$	$1.8 \cdot 10^{-2}$

cross sections over the same mass window are a factor of 600 (respectively, 1600) larger than the Higgs signal but the probability of misidentifying both c jets [respectively, $q(\bar{q})$ jets] as b jets is only of 0.25% (respectively, $2 \cdot 10^{-4}$), and both backgrounds can be further reduced with the same selection criteria applied to remove the $b\bar{b}$ continuum. Note that, in agreement with our leading-order (LO) calculations for the signal, we do not consider the next-to-leading-order (NLO) production of a heavy-quark dijet accompanied by an additional gluon radiated. This process is effectively eliminated by our experimental requirement of two single jets in the event.

Table III lists also the elastic top-antitop continuum inclusive cross section (for all $m_{t\bar{t}}$) which would be an interesting measurement in its own right, although as a potential $H \to b\bar{b}$ background it can be easily removed given the presence of two extra W decays ($t\bar{t} \to b\bar{b}W^+W^-$) in those events. These cross sections should be taken with a grain of salt since the very large $\gamma\gamma$ c.m. energies required ($m_{t\bar{t}} \approx 340$ GeV$/c^2$) are at the limit of applicability of our photon flux approximation.

We obtain a semielastic cross section of continuum b-quark dijets slightly larger (by a factor of $\sim$30%) than the elastic ones. We do not quote the corresponding $c\bar{c}$ and $q\bar{q}$ semielastic cross sections which, for our signal over background studies (Sec. IV D), we take also as a factor of 1.3 larger than the corresponding elastic values.

C. Event rates and pA luminosity considerations

1. pA luminosities

Taken at face value, the results of Fig. 3 indicate that the $\gamma\gamma \to H$ cross section is maximum for lead-lead collisions and thus that this system should be the best suited to carry out such a measurement. Nevertheless, the PbPb luminosity at the LHC is severely limited mostly due to two electromagnetic processes with huge cross sections that affect both Pb beams [67]: (i) electron-positron production followed by e^- capture by one of the nucleus [bound-free pair production (BFPP)], $\mathrm{Pb}^{82+}\mathrm{Pb}^{82+} \xrightarrow{\gamma\gamma} \mathrm{Pb}^{82+}\mathrm{Pb}^{81+}e^+$, with a cross section of $\sigma_{\mathrm{bfpp}} = 280$ b [68], and (ii) Coulomb dissociation of one or both nuclei due to mutual soft photon exchange(s), $^{208}\mathrm{Pb}^{208}\mathrm{Pb} \xrightarrow{\gamma} {}^{208}\mathrm{Pb}^{207}\mathrm{Pb}n$ with a cross section of $\sigma_{\mathrm{emd}} = 215$ b [69]. Both these processes create ions with a magnetic rigidity different than the nominal one for $^{208}\mathrm{Pb}^{82+}$ ions, leading to beam losses and a reduction of the beam lifetime. In addition, the first process poses a danger of LHC magnet quenching due to the large amount of Pb^{81+} ions straying from the nominal beam orbit, impinging on and heating the superconducting dipoles. Although other technical reasons limit the maximum luminosities attainable with ions (see below), BFPP effects effectively reduce the maximum luminosity in PbPb collisions to the $\mathcal{O}(10^{27}$ cm^{-2} s$^{-1})$ range, i.e. 7 order of magnitude below the top pp LHC luminosity, $\mathcal{O}(10^{34}$ cm^{-2} s$^{-1})$.

In pA collisions, the upper theoretical luminosity could be naively taken as the geometric mean of the maximum individual proton and ion beam luminosities, e.g. for pPb, $\mathcal{L}^{\max}_{p\mathrm{Pb}} = \sqrt{\mathcal{L}^{\max}_{\mathrm{Pb}} \cdot \mathcal{L}^{\max}_{p}} = 3 \cdot 10^{30}$ cm^{-2} s^{-1}. However, in principle the Pb-beam luminosities in pPb could be significantly improved compared to PbPb since the $\gamma\gamma \to e^+e^-$ cross section is $Z^2 = 6700$ times smaller and thus the quench limit due to BFPP could be naively raised by a $\mathcal{O}(7000)$ factor of up to $\mathcal{L}^{\max}_{p\mathrm{Pb}} = \sqrt{6700 \cdot \mathcal{L}^{\max}_{\mathrm{Pb}} \cdot \mathcal{L}^{\max}_{p}} = 2 \cdot 10^{32}$ cm^{-2} s^{-1}. This is, however, only an idealistic estimate for several reasons. The beam-beam luminosity in a generic AB collision, $\mathcal{L}_{AB}$, is given by the standard formula

$$\mathcal{L}_{AB} = \frac{N_{b,A} N_{b,B} k_b f_0 \gamma}{4\pi \epsilon_n \beta^*} F(\theta_c, \sigma^*, \sigma_z), \tag{9}$$

where N_b is number of particles (protons or ions) per bunch in each beam, k_b is the number of bunches per beam, $f_0 = 11.246$ kHz is the revolution frequency (given by the LHC radius), γ is the Lorentz factor (the geometric mean of the γ-factors of each beam for asymmetric systems), $\epsilon_n = \sqrt{\gamma^2 - 1}\sigma^2_{x,y}/\beta^*$ is the transverse normalized emittance related to the beam size σ^*, and β^* the optical function at the interaction point (IP). $F(\theta_c, \sigma^*, \sigma_z)$ is a small reduction factor from the half-crossing angle, θ_c, and bunch length σ_z, which we neglect in this discussion. In Table IV we list the beam parameters relevant for the pA running mode [43,44]. We note that, as mentioned in the discussion of Table I, the values quoted are for now only unofficial (but plausible) estimates.

Using these nominal beam parameters[11] and Eq. (9), we obtain the pA luminosities listed in the before-last column of Table IV. The obtained default pPb luminosity is smaller compared to the simple $\mathcal{O}(10^{30}$–10^{32} cm^{-2} s$^{-1})$ estimates given above mainly because, conservatively, the proton intensity is reduced to 10% of its standard value in pp collisions [44]. Note that the number of ions/bunch N_b are significantly lower than the proton ones, mainly because of space charge effects in the SPS, and intrabeam scattering limits at injection in both SPS and LHC.

There are three potential paths to improve the pA luminosity: (i) increase the proton bunch intensity N_b to its standard (10-times higher) value, (ii) increment the number of Pb bunches k_b (which would be possible with the proposed new cryogenic collimators [70]) by a factor of 2–3, and (iii) carry out IP upgrades which should eventually allow factors of two smaller β^* at ATLAS and CMS. All such improvements are not unrealistic given that the time-scale expected for a first proton-nucleus run at the LHC is at least 4–5 years after the first pp operation. By then, the knowledge of the collider and the upgrades

[11] For k_b and ϵ_n one uses the smallest of the proton or nucleus values.

TABLE IV. Basic beam parameters for protons and ions for pA runs at the LHC: particles/bunch N_b, number of bunches k_b, normalized beam emittance ϵ_n, optics β^*, and associated luminosity $\mathcal{L}_{AB}$. Possible upgraded settings (see text) may lead to a factor of 60 improvement of the luminosities (last column).

System	Nominal settings									Upgraded settings
	N_b		k_b		ϵ_n (μm)		β^* (m)		$\mathcal{L}_{AB}$ (cm^{-2} s^{-1})	$\mathcal{L}_{AB}$ (cm^{-2} s^{-1})
	Proton	Ion	Proton	Ion	Proton	Ion	Proton	Ion		
pO (9.9 TeV)	$1.15 \cdot 10^{10}$	$1 \cdot 10^{9}$	2808	592	3.75	1.5	0.5	0.5	$2.7 \cdot 10^{30}$	$1.6 \cdot 10^{32}$
pAr (9.4 TeV)	$1.15 \cdot 10^{10}$	$5.5 \cdot 10^{8}$	2808	592	3.75	1.5	0.5	0.5	$1.5 \cdot 10^{30}$	$1 \cdot 10^{32}$
pPb (8.8 TeV)	$1.15 \cdot 10^{10}$	$7 \cdot 10^{7}$	2808	592	3.75	1.5	0.5	0.5	$1.5 \cdot 10^{29}$	$1 \cdot 10^{31}$

TABLE V. Expected Higgs boson ($m_H = 120$ GeV/c^2) production rates per year N_{Higgs} (in parenthesis those in the $b\bar{b}$ channel) in elastic + semielastic ultraperipheral proton-proton, proton-nucleus, and elastic nucleus-nucleus collisions at the LHC, for two run scenarios (see text). For each system, we quote the corresponding luminosity $\mathcal{L}_{AB}$, the running time Δt, and the average number of overlapping pileup collisions, $\langle N_{\mathrm{pileup}} \rangle$.

System	Nominal runs				Upgraded pA scenario			
	$\mathcal{L}_{AB}$ (cm^{-2} s^{-1})	Δt (s)	$\langle N_{\mathrm{pileup}} \rangle$	N_{Higgs} total ($H \to b\bar{b}$)	$\mathcal{L}_{AB}$ (cm^{-2} s^{-1})	Δt (s)	$\langle N_{\mathrm{pileup}} \rangle$	N_{Higgs} total ($H \to b\bar{b}$)
pp (14 TeV)	10^{34}	10^{7}	25	77 (55)	10^{34}	10^{7}	25	77 (55)
pO(9.9 TeV)	$2.7 \cdot 10^{30}$	10^{6}	0.20	0.022 (0.016)	$1.6 \cdot 10^{32}$	10^{7}	3.9	13 (10)
pAr (9.4 TeV)	$1.5 \cdot 10^{30}$	10^{6}	0.18	0.045 (0.032)	$1 \cdot 10^{32}$	10^{7}	3.6	30 (22)
pPb (8.8 TeV)	$1.5 \cdot 10^{29}$	10^{6}	0.05	0.050 (0.035)	$1 \cdot 10^{31}$	10^{7}	1	34 (25)
PbPb (5.5 TeV)	$5 \cdot 10^{26}$	10^{6}	$5 \cdot 10^{-4}$	0.009 (0.007)	$5 \cdot 10^{26}$	10^{7}	$5 \cdot 10^{-4}$	0.15 (0.1)

related to future LHC projects will be well advanced. The combined effect of such upgrades would optimistically allow one to increase the pA luminosities by a factor of 60 (last column of Table IV).

2. Higgs event rates

The expected number of Higgs bosons expected per year in ultraperipheral pA collisions at the LHC can be obtained, from its production cross section (sum of elastic and inelastic channels) and the time-integrated luminosity, with the standard formula $N = \sigma_H \cdot \mathcal{L}_{AB} \cdot \Delta t$. The nominal LHC running time with protons (respectively, ions) is 8 months (respectively, 1 month) which, with 50% efficiency, corresponds to a run time of $\Delta t \approx 10^7$ (resp. 10^6) s. Using the nominal luminosities quoted in Table IV, we obtain the corresponding expected Higgs events for each one of the systems listed in Table V.

With the default settings and running times, the statistics are marginal for all systems involving nuclei. For the nominal runs, the possibility to carry out a measurement of the Higgs boson in photon-photon collisions at the LHC is virtually null, except maybe for pp if one could work out a trigger—e.g. using forward proton spectrometers [14]—that can deal with the 20 inelastic proton-proton pileup collisions overlapping with the UPC event. A straightforward way to increase the expected yields by a factor of 10 would be to dedicate a full LHC year (10^7 s) to a pA run. This plus the upgraded luminosity settings mentioned above would readily buy one a factor of 600 increase in the expected integrated luminosity (100 pb^{-1}) and, thus, of the number of Higgs counts per year (last column of V). Unavoidably, the proposed improvements of the Pb-beam intensity and $\beta^\star$ optics imply an enhanced probability of having various collisions within the same bunch crossing. The occurrence of event pileup is particularly harmful in the case of UPCs since it eliminates the advantages given by the clean topologies of this type of collisions. The number of overlap collisions can be obtained from the product of the (inelastic[12]) reaction cross section (last column of Table I), the beam luminosity (last column of Table IV) and the mean bunch distance, $\langle N_{\mathrm{pileup}} \rangle = \sigma_{AB} \times \mathcal{L}_{AB} \times \langle \Delta t_{\mathrm{bunch}} \rangle$; the latter parameter depends on the revolution frequency of the beam and the number of bunches, $\langle \Delta t_{\mathrm{bunch}} \rangle = 1/(f_0 k_b)$. In the case of proton-nucleus, running with ions with the nominal bunch filling scheme, the crossing frequency is not well defined as not all encounters will occur at integer multiples of the 100-ns RF frequency [70]. For pPb with $\mathcal{L} = 1.5 \cdot 10^{29}$ cm^{-2} s^{-1}, one has $\langle N_{\mathrm{pileup}} \rangle \sim 0.05$, increasing to ~ 1 if we consider the luminosity upgrades discussed above. Clearly, the pPb system provides the best combination of signal counting rates over pileup probability.

[12]We do not care here about the "harmless" elastic interactions without particle production.

IV. RESULTS II: $H \to b\bar{b}$ MEASUREMENT

In the last section of the paper we consider in detail the possibility to measure a 120 GeV/c^2 Higgs boson produced in ultraperipheral pPb collisions at $\sqrt{s_{NN}} = 8.8$ TeV detected in the dominant $b\bar{b}$ decay channel (BR = 72%) for this mass. Our analysis is entirely based on the ATLAS/CMS detectors (trackers, calorimeters), needed to reconstruct the b jets and confirm the presence of a rapidity gap, at central rapidities ($|\eta| < 2.5$). No additional instrumentation is needed in principle except zero-degree calorimeters to help reduce possible diffractive proton-nucleus interactions (see below). The generator-level rapidity (y) differential distributions for the $H \to b\bar{b}$ signal (histogram) and decay b jets (dashed histogram) are shown in Fig. 4 (the semielastic distribution, not shown, is very similar). In our calculations we take the direction of the proton-beam coming from negative rapidities. We note that the $\gamma\gamma \to H(120\ \text{GeV}/c^2)$ production is peaked forward, at $y = 1.7$ with an rms of ± 1 units of rapidity. On top of the $\Delta y_{\text{c.m.}} = 0.47$ shift due to the asymmetric p and Pb-beam energies, the proton EPA γ spectrum is harder than the Pb one and boosts the production to even larger rapidities. The distribution of the two decay b jets is centered at the parent Higgs rapidity but it is wider (rms of ± 1.4).

The discussion presented hereafter will focus on the ATLAS and CMS experiments which feature b-jet reconstruction capabilities in the range needed to carry out the measurement [shaded (yellow) area in Fig. 4]. The ALICE [25] acceptance for b-jet reconstruction is unfortunately limited to a narrow region $|\eta| < 0.7$ and there are luminosity limitations, $\mathcal{O}(10^{31}\ \text{cm}^{-2}\,\text{s}^{-1})$, linked to the latency of the time-projection-chamber. We do not consider here either the LHCb detector [31], although it features good b-jet identification capabilities at forward rapidities ($\eta \approx 2$–5) and covers a fraction of the Higgs decay acceptance in pPb collisions (provided that the proton-beam direction points in the same direction of the apparatus).

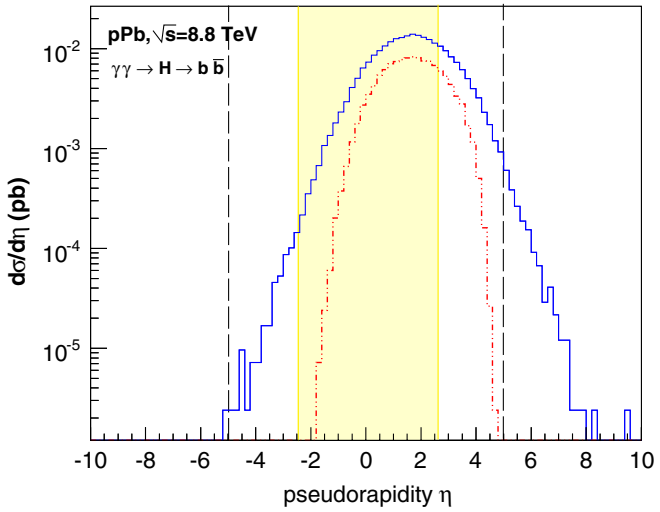

FIG. 4 (color online). Rapidity-differential cross section for a Higgs boson ($m_H = 120\ \text{GeV}/c^2$, dashed histogram) and its decay $b\bar{b}$ jets (histogram) produced in $p\text{Pb} \xrightarrow{\gamma\gamma} p H \text{Pb}$ with $H \to b\bar{b}$. The shaded (yellow) area indicates the acceptance of ATLAS/CMS detectors for b jets. The dashed lines indicate the full acceptance for all other type jets.

In order to obtain realistic estimates of the detectable number of Higgs in the $b\bar{b}$ channel, we have to consider the potential signal losses due to (i) the trigger efficiency (Sec. IV A), (ii) the geometric acceptance of the detectors (Sec. IV B 1), (iii) the inefficiencies introduced by the finite resolution and limitations of the experimental reconstruction (Sec. IV B 2), and (iv) the event selection cuts aiming at removing as much as possible backgrounds (Secs. IV C). We consider in detail these issues in the next subsections.

A. Triggering

There exist detailed trigger studies for ultraperipheral AA collisions at the LHC [18,30]. The main characteristics of (elastic) exclusive two-photon pA events is the production of a single central particle accompanied by large rapidity gaps on both sides of it, and the survival of the interacting proton and nucleus. At variance with ultraperipheral AA collisions, one cannot make use of the zero degree calorimeters (ZDC) [71] to tag the presence of a nucleus radiating a photon in ultraperipheral pA collisions. In AA UPCs, mutual Coulomb excitation of the incoming nuclei due to additional soft photon exchange(s) in the interaction, produce forward neutrons from the decay of the excited nuclear giant-dipole-resonance (GDR) [72]. The GDR excitation probability is proportional to the charge squared of the incoming projectile, which is a factor of $Z^2 \approx 6700$ smaller for a proton than for a lead beam, and very few pPb collisions will be accompanied by forward neutron emission.

For most of the expected pPb beam luminosities where no significant event pileup is expected—i.e. $\langle N_{\text{pileup}} \rangle \lesssim 1$ proton-nucleus collision per bunch crossing—one can easily record ultraperipheral Higgs events with virtually zero signal loss with a level-1 (L1) trigger based e.g. on (i) two back-to-back jets, with at least one of them with $p_T > 40$ GeV/c in the central detector ($|\eta| < 2.5$), accompanied with an exclusivity condition given by (ii) a large rapidity gap $\Delta\eta \gtrsim 2.5$ without hadronic activity along the direction of the ion emitting the exchanged photon (whose energy is softer than the proton one). The rates of all signal and possible backgrounds with such signatures are well below a few Hz, easily allocatable without any prescale within the available L1 bandwidth.

In the semielastic case, only the nucleus survives and the rapidity gap is narrower along the proton direction due to the presence of forward hadrons from the fragmentation of the radiating quark and proton spectator partons. Yet, as discussed previously, our semielastic cross sections have

been computed with the requirement of no activity within $|\eta| < 2.5$ other than the centrally produced system. In addition, since only the proton dissociates the rapidity gap in the Pb direction is unpolluted by any hadronic activity. The event topology of our $H \to b\bar{b}$ semielastic events is basically identical to the pure elastic production and will identically pass the L1 trigger defined above.

For the maximum luminosities, $\mathcal{O}(10^{31}\ \mathrm{cm}^{-2}\,\mathrm{s}^{-1})$, considered in the ''upgraded pA scenario'' one has to account for the possibility of one concurrent pPb collision in the same bunch crossing as the $\gamma\gamma$ interaction (see Table V). In that case the rapidity-gap condition is not necessarily fulfilled since the exclusive event is overlapped by a normal (hadronic) proton-nucleus interaction. One can still use very-forward-proton detectors—like TOTEM [73] and ALFA [74] Roman Pots or the proposed FP420 spectrometer [14]—to tag at the level-2 (L2) trigger, at least, the surviving proton in elastic $\gamma\gamma$ collisions. The nucleus cannot be tagged similarly since its momentum transfer and energy loss are too small to leave the nominal LHC beam envelope. One-side tagging is a standard procedure for triggering on semielastic two-photon events in pp collisions [13]. One can still count on recording UPC events overlapping with a hadronic collision with dedicated level-1 high-p_T b-jet triggers, plus a level-2 single-tagging of a leading proton, and separate offline the two interaction vertices (which is perfectly feasible since ATLAS and CMS can isolate the vertices of 25 overlapping collisions at the highest pp luminosities). In the semielastic case, instead of the leading-proton one can tag the jet issuing from the fragmentation of the radiating quark in the forward calorimeters (FCAL in ATLAS, and HF/CASTOR in CMS). All in all, such a scenario is less straightforward than the one considered for lower luminosities and would deserve a dedicated study beyond the scope of this exploratory paper. For the purpose of this study we will consider that L1 and L2 triggers can be defined in pPb collisions which are fully efficient with respect to the signal with counting rates in the Hz range that do not require any prescale factor.

B. Experimental cuts

Ideally, a complete MC simulation including parton showering and hadronization, full jet reconstruction and GEANT-based detector response, would give fully realistic results for our study. This is, however, beyond the scope of this paper. We can, however, already obtain valid estimates of the feasibility of the measurement taking into account the known basic detector performances, and the kinematical properties of the signal and backgrounds at the generator level.

1. b-jet acceptance

Full jet reconstruction in ATLAS and CMS is possible within $|\eta| < 5$ (or within $|\eta| < 6.6$ in CMS if one includes the CASTOR calorimeter [75]). Jet b-tagging requires however tens of micrometers vertex resolutions to identify the secondary vertex of the decay of the leading B meson of the jet. Such capabilities are present only within the $|\eta| < 2.5$ central tracking coverage of the detectors[13] (see Fig. 4). A realistic ATLAS/CMS cut of the type

(i) both b-jets within $|\eta| < 2.5$,

has an acceptance of 55% (i.e. it leads to a loss of 45% of the signal) for both the elastic and semielastic components. The acceptance for the dominant photon-photon $q\bar{q}$ continuum background (which has a wider distribution, see later) is fortunately smaller (23%). One could in addition displace the vertex of the pPb interaction point along the beam z axis by up to about 0.5 m by adjusting the optics in all experiments without much loss in the luminosity [70]. Such an offset in the proton direction would represent a gain of $\Delta\eta = 0.2$ units of pseudorapidity for b jets, and a corresponding increased geometric acceptance of 60% for $H \to b\bar{b}$.

2. b-jet tagging efficiency

Standard b-jet reconstruction in ATLAS and CMS [7,8] can be tuned to enhance either the b-tagging efficiency or the purity. On the one hand, due to the large charm $\gamma\gamma$ background—with cross sections $e_c^4/e_b^4 = 16$ times larger than $b\bar{b}$—excellent b-tagging (i.e. increased purity) is required. On the other hand, one needs high tagging efficiency since the $b\bar{b}$ reconstruction squares any single b-jet efficiency loss. Studying the ratio $(S/B) \propto \varepsilon^2_{b\text{-tag}} \cdot \sigma_{H\to b\bar{b}}/[\varepsilon^2_{c\text{-mistag}} \cdot \sigma_{c\bar{c}} + \varepsilon^2_{q\text{-mistag}} \cdot \sigma_{q\bar{q}}]$ for various (correlated) (mis)tagging efficiencies from [7,8], leads us to choose a working point of 70% b-jet tagging efficiency and a mistag rate of 5% for c quarks and 1.5% for light-quark and gluon jets. The c-quark mistagging factor is a bit optimistic but it is likely at reach with multivariate-type analyses [76] after a few years of experience with previous pp data. Jet tagging efficiencies are slightly worst in the rapidities beyond $|\eta| \approx 1.5$ (for both signal and background jets), however the low particle multiplicities in two-photon events, likely compensate for such performance losses. In our analysis, we have therefore considered the following η-independent b-jet reconstruction performances:

(i) b-jet tagging efficiency: 70% for a single b jet,
(ii) b-jet mistagging probabilities: 5% for a c quark, and 1.5% for a light quark,

which, for our *double* b-jet events of interest, lead to a $\sim$50% efficiency for the signal and a total reduction of the $c\bar{c}$ and $q\bar{q}$ continuum backgrounds by factors of $\sim$400 and $\sim 4 \cdot 10^5$, respectively.

[13]The combination of the CMS forward HF calorimeters and the TOTEM T1 trackers [73] could potentially help to further extend the coverage for b jets in ''particle-flow''-type analyses.

C. Background rejection

Our ultimate goal is to have a number of Higgs events collected and a signal over background (S/B) which is significant enough to observe the $H \to b\bar{b}$ channel at least at the $S/\sqrt{B} = 3\sigma$ level. We discuss in this section the procedure to remove in an offline analysis any remaining heavy-quark background that could have passed the triggers and experimental cuts discussed above.

1. Hadronic background

There may be peripheral (but still hadronic) grazing pPb collisions with heavy-quark dijet production and wide η ranges without hadronic production (above experimental thresholds) which potentially pass our trigger selection criteria. The very low particle multiplicity and the very small transverse momentum of the centrally produced system ($p_T \approx 0$ at leading order but smeared by the experimental resolution) expected for the very low virtuality of the exchanged photons in UPCs can be successfully used to distinguish them from standard peripheral hadronic interactions:

(i) Jet multiplicity, $N_{\rm jet} = 2$: Requiring just two b jets within $|\eta| < 2.5$ selects with 100% efficiency "clean" exclusive events and removes almost completely any hadronic interaction. This eliminates also possible genuine $\gamma\gamma \to H$ events where an additional jet from hard gluon emission is emitted, but this is consistent with the tree-level cross sections presented in the paper.

(ii) Exclusivity: Absence of hadronic activity (above detector backgrounds) outside the reconstructed jets, within $|\eta| < 2.5$ for tracks and neutral particles. For neutrals, one can extend the rapidity-gap condition in the Pb direction up to $|\eta| < 5$ (or $|\eta| < 6.6$ if one includes the CASTOR calorimeter in CMS), while still saving the semielastic signal.

(iii) Very low transverse momentum of the dijet system: $p_T^{\rm pair} \lesssim 5$ GeV/c. Any photon-photon central system is expected to be produced almost at rest. Selecting events whose net p_T is below a few GeV/c, to account for the experimental reconstruction of a pair of two b jets, eliminates any hadronic collision and still saves the semielastic Higgs component (with $p_T^H < 5$ GeV/c, see Sec. II A 2).

The application, at the offline analysis level, of such cuts removes virtually any remaining peripheral hadronic pPb which could have been recorded at the trigger level, with zero loss of the elastic and semielastic Higgs signals. In addition, if needed, one can also take into account the fact that the hadronic pPb production of $b\bar{b}$ jets is peaked at $y \approx 0.47$ (see Sec. II) whereas the two-photon fusion events are mostly centered at $y \approx 1.7$ (Fig. 4).

2. Diffractive and photoproduction backgrounds

The experimental signatures of central diffractive (Pomeron-Pomeron or Pomeron-photon) interactions—exclusive central object and two rapidity gaps—are very similar to two-photon fusion processes [77]. Central exclusive production of $b\bar{b}$ jets above $p_T \approx 40$ GeV/c ($\mathbb{P}\mathbb{P} \to b\bar{b}$) is a typical background for exclusive Higgs production ($\mathbb{P}\mathbb{P} \to H \to b\bar{b}$) with cross sections of the same order as the Higgs signal itself [14]. Likewise, photoproduction of high-p_T heavy-quarks—in photon-gluon fusion via a t- or u-channel $q\bar{q}$ pair ($\gamma g \to b\bar{b}$) [78,79] or photon-Pomeron [79,80] processes ($\gamma\mathbb{P} \to b\bar{b}$)—have event topologies (survival of the nucleus, one rapidity gap) similar to semielastic $\gamma\gamma$ production, and cross sections in pPb collisions of order of a few nb for b jets above $p_T \approx 40$ GeV/c, the purely diffractive contribution being $\sim$10% of it [79,81].

Though both type of events have cross sections 2 to 3 orders of magnitude larger than our signal and they can potentially pass the trigger cuts and contaminate our signal sample, there are various features that separate $\gamma\gamma$ events from $\mathbb{P}$-induced and γ-gluon, γ-$\mathbb{P}$ events:

(i) Photon-induced interactions are less central (i.e. take place at larger impact parameters) than Pomeron-induced ones and, thus, the corresponding gap-survival probabilities for masses $\mathcal{O}(100\ {\rm GeV}/c^2)$ are much larger. The gap-survival factor for Higgs production in pp collisions at the LHC is $\hat{S}^2_{\gamma\gamma} = 0.9$ in photon-fusion compared to $\hat{S}^2_{\mathbb{P}\mathbb{P}} = 0.03$ in Pomeron-fusion [9]. In the case of proton-nucleus collisions, the situation is comparably much more favorable for electromagnetic Higgs production: $\hat{S}^2_{\gamma\gamma} = 0.85$ versus $\hat{S}^2_{\mathbb{P}\mathbb{P}} = 8 \cdot 10^{-4}$ [82].

(ii) Since the nucleus is a fragile object—the binding energy of a nucleon is just 8 MeV—even the softest Pomeron-mediated interactions will result in the emission of a few nucleons from the ion, detectable in the zero-degree calorimeters. On the contrary, in purely electromagnetic pA interactions both hadrons remain intact after the interaction and no other forward particles are emitted.

(iii) The net p_T of elastic $\gamma\gamma$ final states is zero at LO. In the semielastic case, the typical p_T of the produced Higgs is peaked below 1 GeV/c. In both cases, the total net p_T is thus smaller than for comparable γ-nucleus or γ-proton interactions and thus is also an effective tool for separating the two classes of interactions [51].

(iv) Because of the larger nucleus flux, heavy-quark photoproduction in pPb is dominated by collisions of photons emitted by the lead nucleus with a gluon ($\gamma_{\rm Pb} g_p$) or Pomeron ($\gamma_{\rm Pb}\mathbb{P}_p$) that carry a larger fraction of the 7-TeV proton-beam energy. The produced particles will be thus more forward

boosted than our signal which comes from $\gamma_{\mathrm{Pb}}\gamma_p$ collisions.

In short, inclusive high-p_T heavy-quark photon- and Pomeron-induced production will partially fill one or both rapidity gaps and/or be accompanied by zero-degree neutrons, and the purely exclusive production for both processes has a gap-survival probability below 10^{-3}. Thus, already before any kinematics cuts, both backgrounds are (much) smaller than our signal.

High-p_T heavy-quark production can also take place via single (or double) resolved processes with very energetic photons which interact via their partonic content [83] in collisions where the proton and the nucleus come very close together. We disregard this contribution in this analysis for various reasons. First, although the effective two-photon luminosity has indeed a large tail (Fig. 2), the photon fluxes are exponentially decreasing and the contributions to the cross sections in the high-$W_{\gamma\gamma}$ region relevant for such resolved processes are very small. Second, the much more energetic photon flux of the proton could be potentially resolved but at the price of an interaction so close (with an impact parameter b likely smaller than $R_p + R_{\mathrm{Pb}}$) that the nucleus would break apart after the interaction. Our requirement for an intact nucleus implicitly sets a limit on the probability to resolve the photon. Last but not least, any potential resolved photon contribution, would not only contribute to the heavy-quark background but also to the Higgs signal itself [84].

3. Photon-photon continuum backgrounds

The only physical backgrounds to $H \to b\bar{b}$ in electromagnetic pPb collisions are the (elastic and semielastic) exclusive $\gamma\gamma \to Q\bar{Q}$, $q\bar{q}$ processes with the cross sections[14] quoted in Table III. Other two-photon fusion processes, such as $\gamma\gamma \to \tau^+\tau^-$ or $\gamma\gamma \to t\bar{t}$ (see Table III), have final states (e.g. particle multiplicities) different than Higgs decay into two b jets. Although important (see Fig. 5), the irreducible heavy-quark dijet backgrounds can be suppressed with various kinematics cuts.

First, the continuum can be reduced if we require the b-jet transverse momentum to be bigger than a significant fraction of the $b\bar{b}$ invariant mass. In Fig. 6 (left panel), we compare the p_T distribution of the signal and background before cuts. The background is dominated by one jet with low p_T (but large p_L), whereas the signal peaks at $p_T \approx m_H/2 = 60$ GeV/c. Selecting events where there is at least one jet with $p_T = 52$–60 GeV/c removes 96% (97%) of the $b\bar{b}$ ($c\bar{c}$) background while killing only 49% of the signal. Second, whereas the two Higgs decay b jets are emitted isotropically, the continuum—whose relevant Feynman diagrams have quarks propagating in the t- or u-channel—is peaked in the forward and backward directions (Fig. 7). Cutting on the angle θ between the b jet (boosted to the rest frame of the pair[15]) and the direction of the pair (helicity frame[16]) removes an important fraction of the background. The b jets from the continuum are clearly peaked at $|\cos\theta| \approx 1$, i.e. emitted either roughly in the same direction as the pair or opposite to it. With a rather strict $|\cos\theta| < 0.45$ cut, 82% of the continuum is suppressed for a 55% signal loss.

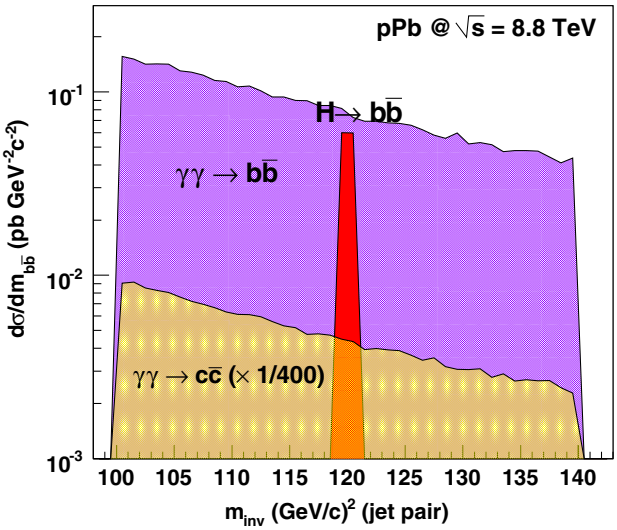

FIG. 5 (color online). Invariant mass distribution of pairs of b jets from: (i) $H \to b\bar{b}$ events and (ii) $\gamma\gamma \to b\bar{b}$ and $c\bar{c}$ (misidentified with 0.25% probability) continuum, in ultraperipheral pPb collisions at 8.8 TeV. The Higgs peak is plotted with an (arbitrary) $\Delta m_H = 1$ GeV/c^2 width.

Other cuts were tested, based e.g. on the rapidity separation $|y_b - y_{\bar{b}}|$ between jets, without further background suppression power. The final set of cuts applied in our analysis is thus

(i) Transverse momentum: at least one jet with p_T^{jet} between $m_H/2.3 = 52$ GeV/c and the kinematical limit at $m_H/2 = 60$ GeV/c.
(ii) Acollinearity: $|\cos\theta| < 0.45$, where θ is the helicity-frame angle (between the b jet, boosted to the rest frame of the pair, and the direction of the pair).
(iii) Mass window: Invariant mass of the b-jet pairs around the Higgs mass: $m_{\mathrm{pair}} = 100$–140 GeV/c^2 (the range given by 2 or 3 times the width of experimental mass resolution).

We note that for a given event, these selection criteria (as well as the previous acceptance and b-tagging efficiency cuts) do not necessarily factorize.

[14]The semielastic $c\bar{c}$ and $q\bar{q}$ continuum are taken to be 1.3 times the corresponding elastic cross sections as found in the $b\bar{b}$ case.

[15]The $\bar{b}$ jet is at π rads from it.

[16]One can use alternatively the Gottfried-Jackson frame, which uses the direction of the beam. The results are unchanged.

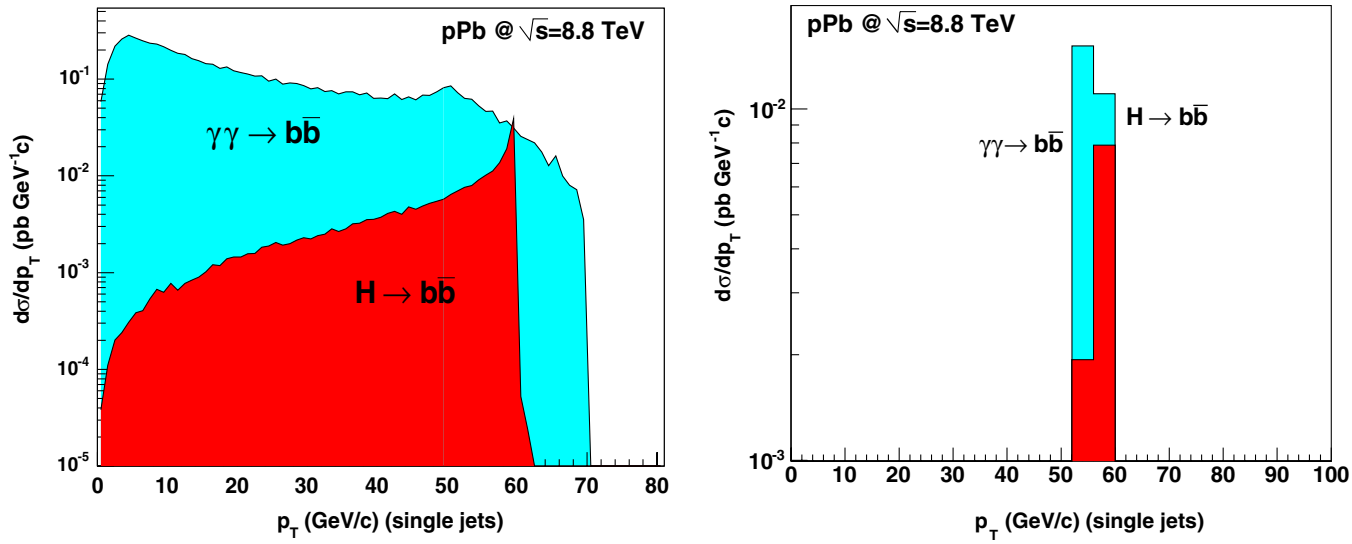

FIG. 6 (color online). Transverse momentum distribution of single b jets from $H \to b\bar{b}$ and $\gamma\gamma \to b\bar{b}$ continuum events in ultraperipheral pPb collisions at 8.8 TeV, before (pure MC-level, left panel) and after (right panel) applying all the experimental cuts discussed in the text.

D. Signal significance

The combined application of all experimental and background suppression cuts discussed in the previous section leads to a loss of about 80% of the Higgs events and an important reduction of the $b\bar{b}$, $c\bar{c}$, and $q\bar{q}$ continuum backgrounds by factors of 60, 5000, and $4 \cdot 10^5$, respectively. In one year (10^7 s) with the upgraded 10^{31} cm^{-2} s^{-1} pA luminosity scenario (i.e. integrating 100 pb^{-1} of luminosity) this corresponds to a collection of $N = 5$ Higgs and $N = 10$ $b\bar{b}$ continuum events within 100–140 GeV/c^2 with small $c\bar{c}$ ($N = 0.16$) and negligible $q\bar{q}$ contributions. These values include both elastic and semielastic processes for the signal and backgrounds. The continuum decreases exponentially in this mass range whereas the Higgs signal peaks at $m_H = 120$ GeV/c^2.

In order to determine the significance of our $H \to b\bar{b}$ signal, we generate event samples consisting of the appropriate number of events after cuts in 3 years ($3 \cdot 10^7$ s) of data taking, i.e. 300 pb^{-1} of integrated luminosity, with a fast Monte Carlo. We assume a $b\bar{b}$ dijet invariant mass resolution of 7 GeV/c^2. Such a value is beyond the current performances for b jets in the range $p_T = 50$–60 GeV/c,

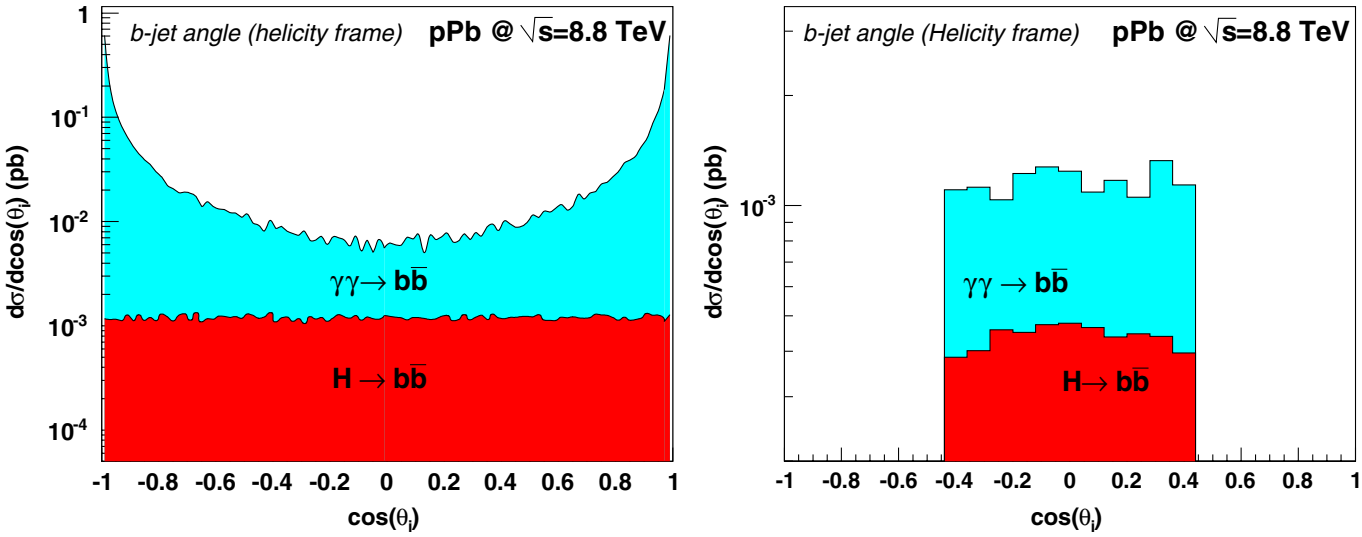

FIG. 7 (color online). Distribution of $\cos(\theta)$ for b jets in the helicity frame from (i) $\gamma\gamma \to b\bar{b}$ continuum (top histograms) and (ii) $H \to b\bar{b}$ signal (bottom histograms) in ultraperipheral pPb collisions at 8.8 TeV, before (pure MC-level, left panel) and after (right panel) applying all the experimental cuts discussed in the text.

but may be achieved, in our underlying-event-free environment, with particle-flow reconstruction techniques and a good data-based knowledge of the b-jet p_T resolution and energy scale after a few years of LHC running. We then perform a log-likelihood fit to the pseudodata with two curves: (i) one assuming that there is a signal + continuum in the region $100 \leq m_H \leq 140$ GeV$/c^2$, and (ii) one assuming that there is just continuum. The significance, S, is then given by

$$\mathcal{S} = \sqrt{\Delta\chi^2}, \tag{10}$$

where $\Delta\chi^2$ is the difference of the χ^2 of the fits for the signal and null hypotheses. We fit the peak region using a Gaussian fixed at $m_H = 120$ GeV$/c^2$ (the Higgs mass, if any, will be already known by the time this measurement can be carried out) with width $\Delta m_H = 7$ GeV$/c^2$ to match the assumed experimental mass resolution. We consider that the shape of the background will be known, since it can be measured with high statistics by simply removing the kinematics cuts applied to enhance the Higgs signal. According to our simulations, the exclusive continuum after cuts can be well reproduced by an exponential distribution with inverse slope $[28\ \text{GeV}/c^2]^{-1}$, which we also fix in our fit. The normalization of the signal and background are left as the only two free fit parameters. We repeat this method for 500 pseudodata sets to obtain the average significance of the fits. An example of a typical pseudodata set and fits is shown in Fig. 8. The error bars correspond to $\sqrt{N}$ statistical errors. For a total integrated luminosity of 300 pb^{-1}, we reach a signal-to-background ratio of $S_{H\to b\bar{b}}/B_{\gamma\gamma\to b\bar{b}} \approx 1.5$ and a statistical significance of $\mathcal{S} \approx 3$.

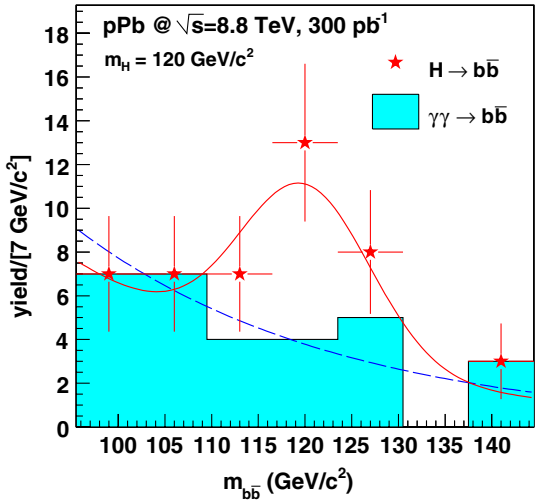

FIG. 8 (color online). Expected invariant mass distribution after 3 years of pPb running at $\sqrt{s_{NN}} = 8.8$ TeV (300 pb^{-1}) for a $H \to b\bar{b}$ signal and residual $\gamma\gamma \to b\bar{b}$ continuum (histogram) after analysis cuts, fitted to a Gaussian + Exponential distribution (solid line). The data points are the sum of signal + background. The error bars are just statistical. The dashed line shows an exponential fit of the continuum alone.

The main motivation for such a measurement is the unique observation of the SM $H \to b\bar{b}$ decay which seems otherwise unaccessible at the LHC. In addition, the observation of the $\gamma\gamma \to H$ process will provide an independent measurement of the Higgs-γ coupling, likely measured before in the $H \to \gamma\gamma$ discovery channel. The $\gamma\gamma$-Higgs cross section is generated at the one-loop level by all heavy charged particles (W and top-quark in the SM) and it is thus sensitive to possible contributions of charged particles predicted in various extensions of the SM: e.g. chargino and top-squark loops in SUSY models, and/or charged Higgs bosons in general 2-Higgs doublet models (2HDMs). Last but not least, in the minimal SUSY extension of the SM—which predicts three neutral Higgs bosons: the light CP-even h, the heavy CP-even H, and the CP-odd A—the properties of the of h boson for large A masses, are similar to the SM Higgs boson and it could be detected in the $b\bar{b}$ decay mode as described in this work too. A dedicated study will be carried out to check the feasibility of such a measurement.

V. SUMMARY

We have presented a detailed study of the exclusive production of the SM Higgs boson in electromagnetic (ultraperipheral) proton-nucleus collisions at the LHC. We have evaluated the production cross sections and the corresponding yields via two-photon fusion processes in elastic ($p\text{Pb} \xrightarrow{\gamma\gamma} pH\text{Pb}$) and semielastic ($p\text{Pb} \xrightarrow{\gamma\gamma} XH\text{Pb}$) reactions, the latter being characterized by the breaking of the proton in the very forward region. Such a measurement can be used to study, on the one hand, the $H - b$ coupling which is otherwise not accessible to measurement at the LHC and, on the other, the photon-photon coupling to the Higgs, i.e. provides an independent check of the previously measured $H \to \gamma\gamma$ decay.

First, we have computed the Higgs boson cross sections in ultraperipheral pp, pA and PbPb collisions at LHC energies with the MADGRAPH Monte Carlo supplemented with equivalent photon spectra, and demonstrated that pPb collisions at $\sqrt{s_{NN}} = 8.8$ TeV give the best potential for such studies when realistic reachable luminosities and event pileup issues are considered. In such a case, the total cross section of a Higgs boson of $m_H = 120$ GeV$/c^2$ is about 0.15 pb for both elastic and semielastic cases. The irreducible background due to the exclusive heavy-quark (and possibly misidentified light-quark) pair continuum, $\gamma\gamma \to Q\bar{Q}$, $q\bar{q}$ has been also computed, along with the elastic $t\bar{t}$ production cross section, for electromagnetic pAr, pO and pPb collisions.

In order to determine the feasibility of the $H \to b\bar{b}$ measurement, we have proceeded to a detailed evaluation of the trigger setup needed, as well as the acceptances and efficiencies for the signal and continuum, and determined

the best set of kinematical cuts needed to maximize the signal over background ratio. With reachable b-jet experimental reconstruction performances, we have found that a Higgs boson with $m_H = 120\ \mathrm{GeV}/c^2$ could be observed in the $b\bar{b}$ channel with a 3σ-significance integrating $300\ \mathrm{pb}^{-1}$ with an upgraded pA luminosity of $10^{31}\ \mathrm{cm}^{-2}\,\mathrm{s}^{-1}$.

To conclude, while such a study will be rather demanding in terms of luminosity, we have shown that it offers a unique complementary potential to the standard Higgs production mechanisms with regards to the study of its couplings to b-quarks and photons at the LHC. Both measurements are key to constrain the standard model and any of its possible extensions.

ACKNOWLEDGMENTS

We thank Stan Brodsky, Albert de Roeck, Michael Peskin, and Mark Strikman for valuable discussions and suggestions on the paper. We also thank Johan Alwall, Gerhard Baur, Rikkert Frederix, John Jowett, Valery Khoze, Bernard Pire, Florian Schwennsen, and Ramona Vogt for useful communications. D. d'E. acknowledges support by the 7th EU Framework Programme (Contract No. FP7-ERG-2008-235071). This work is supported in part by the Belgian American Educational Foundation, the Francqui Foundation and the U.S. Department of Energy under Contract No. DE-AC02-76SF00515.

[1] F. Englert and R. Brout, Phys. Rev. Lett. **13**, 321 (1964); P. W. Higgs, Phys. Rev. Lett. **13**, 508 (1964).
[2] R. Barate *et al.* (LEP Working Group for Higgs Boson Searches), Phys. Lett. B **565**, 61 (2003).
[3] LEP-Tevatron-SLD Electroweak Working Group, arXiv:0811.4682.
[4] A. Djouadi, Phys. Rep. **457**, 1 (2008).
[5] A. De Roeck and G. Polesello, C. R. Physique **8**, 1078 (2007).
[6] J. M. Butterworth, A. R. Davison, M. Rubin, and G. P. Salam, Phys. Rev. Lett. **100**, 242001 (2008).
[7] G. Aad *et al.* (ATLAS Collaboration), arXiv:0901.0512.
[8] G. L. Bayatian *et al.* (CMS Collaboration), J. Phys. G **34**, 995 (2007).
[9] V. A. Khoze, A. D. Martin, and M. G. Ryskin, Eur. Phys. J. C **23**, 311 (2002).
[10] A. De Roeck, V. Khoze, A. D. Martin, R. Orava, and M. G. Ryskin, Eur. Phys. J. C **25**, 391 (2002).
[11] K. Piotrzkowski, Phys. Rev. D **63**, 071502 (2001).
[12] *Proceedings of the International Workshop on High-Energy Photon Collisions at the LHC*, edited by D. d'Enterria, M. Klasen, and K. Piotrzkowski [Nucl. Phys. B, Proc. Suppl. 179, 1 (2008)].
[13] J. de Favereau *et al.*, arXiv:0908.2020.
[14] M. G. Albrow *et al.* (FP420 R&D Collaboration), JINST **4**, T10001 (2009).
[15] C. A. Bertulani, S. R. Klein, and J. Nystrand, Annu. Rev. Nucl. Part. Sci. **55**, 271 (2005).
[16] C. von Weizsäcker, Z. Phys. **88**, 612 (1934); E. J. Williams, Phys. Rev. **45**, 729 (1934); E. Fermi, Nuovo Cimento **2**, 143 (1925).
[17] S. J. Brodsky, T. Kinoshita, and H. Terazawa, Phys. Rev. Lett. **25**, 972 (1970); Phys. Rev. D **4**, 1532 (1971).
[18] A. Baltz *et al.*, Phys. Rep. **458**, 1 (2008).
[19] A. Afanasiev *et al.* (PHENIX Collaboration), Phys. Lett. B **679**, 321 (2009); D. d'Enterria, arXiv:nucl-ex/0601001.
[20] C. Adler *et al.* (STAR Collaboration), Phys. Rev. Lett. **89**, 272302 (2002).
[21] J. Adams *et al.* (STAR Collaboration), Phys. Rev. C **70**, 031902 (2004).
[22] A. Abulencia *et al.* (CDF Collaboration), Phys. Rev. Lett. **98**, 112001 (2007).
[23] T. Aaltonen *et al.* (CDF Collaboration), Phys. Rev. Lett. **102**, 222002 (2009).
[24] T. Aaltonen *et al.* (CDF Collaboration), Phys. Rev. Lett. **102**, 242001 (2009).
[25] F. Carminati *et al.* (ALICE Collaboration), J. Phys. G **30**, 1517 (2004).
[26] B. Alessandro *et al.* (ALICE Collaboration), J. Phys. G **32**, 1295 (2006).
[27] O. Kepka and C. Royon, Nucl. Phys. B, Proc. Suppl. **179–180**, 265 (2008).
[28] V. Pozdnyakov (ATLAS Collaboration), Nucl. Phys. B, Proc. Suppl. **184**, 180 (2008); S. White, Acta Phys. Hung. A **25**, 531 (2006).
[29] M. Albrow *et al.* (CMS and TOTEM Collaborations), CERN/LHCC, Report No. 2006-039/G-124.
[30] D. d'Enterria *et al.* (CMS Collaboration), J. Phys. G **34**, 2307 (2007).
[31] R. Antunes *et al.* (LHCb Collaboration), Report No. CERN-LHCC-2003-030;
[32] J. Anderson and R. McNulty, Report No. LHCb-2008-001.
[33] G. Baur, K. Hencken, D. Trautmann, S. Sadovsky, and Y. Kharlov, Phys. Rep. **364**, 359 (2002).
[34] E. Papageorgiu, Phys. Lett. B **352**, 394 (1995).
[35] M. Grabiak, B. Muller, W. Greiner, G. Soff, and P. Koch, J. Phys. G **15**, L25 (1989).
[36] E. Papageorgiu, Phys. Rev. D **40**, 92 (1989).
[37] M. Drees, J. R. Ellis, and D. Zeppenfeld, Phys. Lett. B **223**, 454 (1989).
[38] J. S. Miller, arXiv:0704.1985.
[39] A. J. Baltz and M. Strikman, Phys. Rev. D **57**, 548 (1998).
[40] A. Kryukov and L. Sarycheva, Nucl. Phys. B, Proc. Suppl. **179–180**, 285 (2008).
[41] J. R. Cudell *et al.* (COMPETE Collaboration), Phys. Rev. Lett. **89**, 201801 (2002).
[42] D. d'Enterria, arXiv:nucl-ex/0302016.
[43] C. A. Salgado *et al.*, "Proton-nucleus at the LHC: Scientific opportunities and requirements" (unpublished).

[44] J. Jowett and C. Carli, in *Proceedings of the Tenth European Particle Accelerator Conference, Edinburgh, 2006*, p. 550, http://accelconf.web.cern.ch/AccelConf/e06/.
[45] N. Armesto *et al.*, J. Phys. G **35**, 054001 (2008).
[46] A. Accardi *et al.*, arXiv:hep-ph/0308248.
[47] V. M. Budnev, I. F. Ginzburg, G. V. Meledin, and V. G. Serbo, Phys. Rep. **15**, 181 (1975).
[48] R. N. Cahn and J. D. Jackson, Phys. Rev. D **42**, 3690 (1990).
[49] G. Baur and L. G. Ferreira Filho, Nucl. Phys. **A518**, 786 (1990).
[50] J. D. Jackson, *Classical Electrodynamics* (John Wiley & Sons, New York, 1975), 2nd ed..
[51] A. J. Baltz, Y. Gorbunov, S. R. Klein, and J. Nystrand, Phys. Rev. C **80**, 044902 (2009).
[52] B. Pire, F. Schwennsen, L. Szymanowski, and S. Wallon, Phys. Rev. D **78**, 094009 (2008).
[53] J. Alwall *et al.*, J. High Energy Phys. 09 (2007) 028.
[54] B. A. Kniehl, Phys. Lett. B **254**, 267 (1991).
[55] J. Nystrand, Nucl. Phys. **A752**, 470 (2005).
[56] R. N. Cahn, in *Proceedings of the XIVth International Symposium on Lepton and Photon Interactions, Stanford California, 1989*, edited by M. Riordan (World Scientific, Singapore, 1989), p. 60.
[57] I. Sick, Phys. Lett. B **576**, 62 (2003).
[58] C. Diaconu, *Proceedings of 15th International Workshop on Deep-Inelastic Scattering and Related Subjects (DIS 2007), Munich, 2007* [Progress in High Energy Physics 1, 2 (2007)].
[59] M. Drees, R. M. Godbole, M. Nowakowski, and S. D. Rindani, Phys. Rev. D **50**, 2335 (1994).
[60] J. Ohnemus, S. Rudaz, T. F. Walsh, and P. M. Zerwas, Phys. Lett. B **334**, 203 (1994).
[61] G. Bhattacharya, P. Kalyniak, and K. A. Peterson, Phys. Rev. D **53**, 2371 (1996).
[62] J. Ohnemus, T. F. Walsh, and P. M. Zerwas, Phys. Lett. B **328**, 369 (1994).
[63] M. Gluck, M. Stratmann, and W. Vogelsang, Phys. Lett. B **343**, 399 (1995).
[64] J. Pumplin, D. R. Stump, J. Huston, H. L. Lai, P. M. Nadolsky, and W. K. Tung, J. High Energy Phys. 07 (2002) 012.
[65] M. A. Shifman, A. I. Vainshtein, M. B. Voloshin, and V. I. Zakharov, Yad. Fiz. **30**, 1368 (1979) [Sov. J. Nucl. Phys. **30**, 711 (1979)]; B. A. Kniehl and M. Spira, Z. Phys. C **69**, 77 (1995); S. Dawson and R. Kauffman, Phys. Rev. D **49**, 2298 (1994).
[66] A. Djouadi, J. Kalinowski, and M. Spira, Comput. Phys. Commun. **108**, 56 (1998).
[67] J. M. Jowett, J. Phys. G **35**, 104028 (2008).
[68] H. Meier, Z. Halabuka, K. Hencken, D. Trautmann, and G. Baur, Phys. Rev. A **63**, 032713 (2001).
[69] I. A. Pshenichnov, J. P. Bondorf, I. N. Mishustin, A. Ventura, and S. Masetti, Phys. Rev. C **64**, 024903 (2001).
[70] J. M. Jowett (private communication).
[71] O. A. Grachov *et al.* (CMS Collaboration), AIP Conf. Proc. **867**, 258 (2006); S. N. White *et al.* (ATLAS Collaboration), Report No. CERN-LHCC-2007-001.
[72] C. A. Bertulani and G. Baur, Phys. Rep. **163**, 299 (1988).
[73] V. Berardi *et al.* (TOTEM Collaboration), Report No. CERN/LHCC-2004-002, 2004.
[74] S. Ask, *Proceedings of 15th International Workshop on Deep-Inelastic Scattering and Related Subjects (DIS 2007), Munich, 2007* [Progress in High Energy Physics 1, 97 (2007)].
[75] X. Aslanoglou *et al.*, Eur. Phys. J. C **52**, 495 (2007).
[76] C. Saout, Proc. Sci., ACAT08 (2008) 101.
[77] R. Engel, M. A. Braun, C. Pajares, and J. Ranft, Z. Phys. C **74**, 687 (1997).
[78] M. Vidovic, M. Greiner, and G. Soff, Mod. Phys. Lett. A **10**, 2471 (1995).
[79] M. Strikman, R. Vogt, and S. N. White, Phys. Rev. Lett. **96**, 082001 (2006).
[80] V. P. Goncalves and M. V. T. Machado, Phys. Rev. D **75**, 031502 (2007).
[81] R. Vogt (private communication).
[82] E. Levin and J. Miller, arXiv:0801.3593.
[83] M. Drees and R. M. Godbole, J. Phys. G **21**, 1559 (1995).
[84] M. A. Doncheski and S. Godfrey, Phys. Rev. D **67**, 073021 (2003).